Chemical Engineering Science 64 (2009) 1416 – 1435

Contents lists available at ScienceDirect

Chemical Engineering Science

journal homepage: www.elsevier.com/locate/ces

A qualitative computational study of mass transfer in upward bubble train flow through square and rectangular mini-channels

Alexandru Onea[a], Martin Wörner[a,*,1], Dan G. Cacuci[b]

[a]Forschungszentrum Karlsruhe, Institut für Reaktorsicherheit, Postfach 3640, 76021 Karlsruhe, Germany
[b]Institut für Kerntechnik und Reaktorsicherheit, Universität Karlsruhe, 76131 Karlsruhe, Germany

ARTICLE INFO

Article history:
Received 8 May 2008
Received in revised form 24 October 2008
Accepted 10 November 2008
Available online 25 November 2008

Keywords:
Simulation
Interface
Multiphase flow
Taylor flow
Mass transfer
Chemical reaction

ABSTRACT

In this paper we present a new method for numerical simulation of conjugate mass transfer of a dilute species with resistance in both phases and an arbitrary equilibrium distribution coefficient. The method is based on the volume-of-fluid technique and accounts for the concentration jump at the interface by transforming the discontinuous physical concentration field into a continuous numerical one. The method is validated by several test problems and is used to investigate the mass transfer in upward bubble train flow within square and rectangular channels. Computations are performed for a single flow unit cell and a channel hydraulic diameter of 2 mm. The simulations consider the transfer of a dilute species from the dispersed gas into the continuous liquid phase. Optionally, the mass transfer is accompanied by a first-order homogeneous chemical reaction in the liquid phase or a first-order heterogeneous reaction at the channel walls. The results of this numerical study are qualitative in nature. First, because periodic boundary conditions in axial direction are not only used for the velocity field but also for the concentration field and second, because the species diffusivity in the liquid phase is arbitrarily increased so that the liquid phase Schmidt number is 0.8 and the thickness of the concentration and momentum boundary layer is similar. Two different equilibrium distribution coefficients are considered, one where the mass transfer is from high to low concentration, and one where it is vice versa. The numerical study focuses on the influence of the unit cell length, liquid slug length and channel aspect ratio on mass transfer. It is found that for the exposure times investigated the liquid film between the bubble and the wall is saturated and the mass transfer occurs by the major part through the bubble front and rear so that short unit cells are more efficient for mass transfer. Similar observations are made for the homogeneous reaction and for the heterogeneous reaction when the reaction is slow. In case of a fast heterogeneous reaction and when the main resistance to mass transfer is in the gas phase, it appears that for square channels long unit cells are more efficient, while large aspect ratio rectangular channels are more efficient than square channels, suggesting that for these conditions they might be more appropriate for use in monolithic catalysts.

1. Introduction

Within the context of process intensification significant interest has been focused in the last decade on investigating the flow in miniaturized devices for microprocess engineering. For multiphase flow applications, e.g. in microstructured reactors (Hessel et al., 2005) and monolithic reactors (Kreutzer et al., 2005), one of the most important advantage as compared to devices of conventional size is the large interfacial area per unit volume that allows high transfer rates between the phases. For a proper design of such miniaturized reactors, the mass transfer phenomena in two-phase flows should be investigated in detail. The difficulties and limitations of experimental methods give the motivation to obtain an insight into mass transfer phenomena across fluid interfaces by numerical simulations.

The numerical investigation of mass transfer can be performed by essentially two different methods. The first approach, which is also employed in this paper, considers the *direct* solution of the species conservation equation while the flow field, needed for convective mass transfer, is obtained by solving the Navier–Stokes equations in both phases. The motion of the interface is considered by means of an interface "tracking" or "capturing" method. This direct approach does not involve any empirical models for the mass transfer coefficient or other closure assumptions and can in principle be applied to

* Corresponding author. Tel.: +49 7247 82 4477; fax: +49 7247 82 4837.
E-mail address: martin.woerner@iket.fzk.de (M. Wörner).
[1] Present address: Forschungszentrum Karlsruhe, Institut für Kern- und Energietechnik, Postfach 3640, 76021 Karlsruhe, Germany.

0009-2509/$ - see front matter © 2008 Elsevier Ltd. All rights reserved.
doi:10.1016/j.ces.2008.11.008

any interfacial geometry and to any two-phase flow topology. However, it requires sufficiently fine grids and sufficiently small time steps so that all spatial and temporal scales of both the concentration and the flow field are well resolved. Therefore, the computational time is generally large and the method is currently restricted to fundamental investigations of scientific interest. In the second *indirect* approach one does not solve the local equations. Instead, to save CPU time, one uses averaged equations, such as in the Euler–Euler model, or one assumes that the two-phase flow consists of disperse elements of presumed shape such as in the Euler–Lagrange model. Both methods are widely used for engineering purposes. However, their generality is restricted since they always rely on certain assumptions for mass transfer and/or hydrodynamics and thus require appropriate closure models. While such models are traditionally developed on the basis of analytical methods and well defined experiments, the direct simulation method is nowadays emerging as a valuable additional tool for this purpose.

The direct numerical simulation of mass transfer for flows, where the shape of the deforming interfaces is part of the solution, is associated with three major difficulties. The first one is related to the Schmidt number (Sc) in the liquid phase which is usually large and of order 1000. In this case, the relative motion between the phases leads to a very thin concentration boundary layer whose thickness is much smaller than that of the momentum boundary layer. Thus, the concentration boundary layer determines the grid size of the numerical computation. As a consequence direct numerical simulations become very CPU time demanding for large values of Sc. If the gas phase consists of a pure substance which dissolves into the liquid phase, then it is sufficient to solve only for the concentration in the liquid phase with an appropriate constant concentration prescribed at the interface. In microfluidic applications, the gas phase often consists of two species, one that can be considered as inert and one that undergoes the mass transfer, e.g. N_2 with 10% F_2 (Hessel et al., 2005). The same applies for droplet flows formed by two immiscible fluids where a dissolved third component transfers from one liquid to the other. In such cases the resistance to mass transfer in the disperse phase cannot be neglected since concentration boundary layers form at both sides of the interface. This leads to the second difficulty, namely the necessity to solve the concentration fields in and outside of the disperse elements simultaneously. Related to this is the third difficulty, which arises from thermodynamics. In general, the concentrations on both sides of the interface are not continuous. There are numerous definitions for the coefficient in Henry's law to quantify this jump at equilibrium (Sander, 1999). In this paper we will use the ratio at equilibrium between the liquid-phase concentration of a species and its gas-phase concentration and denote this dimensionless quantity as Henry number H. Depending on the system, H can vary from 10^{-3} to 10^{15} (Sander, 1999). This requires special numerical measures, which will be discussed below.

The first numerical simulations of mass transfer coupled with the volume-of-fluid (VOF) method for interface tracking are reported by Ohta and Suzuki (1996). Their study of mass transfer from a rising drop in a solvent extraction process was restricted to the simple case where the species concentration and the diffusivity on both sides of the interface were continuous. In their axi-symmetric computations on a uniform grid the drop diameter is resolved by 16 mesh cells. While they considered three values of the Schmidt number ($Sc = 10$, 100, 1000) is it clear that the spatial resolution is, at least for the two higher values of Sc, insufficient to resolve the concentration boundary layer. A VOF method with mass transfer is also described by Davidson and Rudman (2002), who calculated the mass transfer from a drop rising in a liquid column for conditions when the main resistance to mass transfer is in the drop phase. Also in this method continuity of the concentrations at the interface is assumed. Sato et al. (2000) used a marker-density function method together with a total variation-diminishing scheme to perform three-dimensional simulations of the dissolution of a droplet consisting of liquid CO_2 rising in water. The dissolved mass concentration equation is solved only in the continuous phase ($Sc = 1$), while the dissolution flux is given at the interface as boundary condition. Petera and Weatherley (2001) investigated the mass transfer from a falling axisymmetric drop using a finite element approach which employs an automatic remeshing procedure close to the interface. Though the Schmidt number in the continuous phase is very high ($Sc \approx 10^4$), they reported good agreement between the numerical solution and experimental data for the extraction of ethanol from an ethanol–water mixture into a n-decanol solution. They found that the mass transfer is affected by the internal recirculation within the drop and by the recirculation zone in the continuous phase, while the concentration wake is smooth, symmetrical and regular. The finite element method was also used by Waheed et al. (2002) to compute the mass transfer of single spherical drops by free and forced convection. The computations are performed for $Re \leqslant 20$ with $Sc \approx 1000$ in the continuous phase, while the Henry number is set to unity and the size of the drop is assumed constant. Bothe et al. (2003, 2004) reported three-dimensional numerical simulations of oxygen transfer from single air bubbles with Schmidt number ranging from 1 to 1000 and from two-dimensional simulations of a train of air bubbles rising within aqueous solutions. Nevertheless, it is stated that relevant results for mass transfer can be achieved with today's computational power only for Schmidt numbers up to around 100. The concentration field is considered discontinuous at the interface, with the concentration jump being defined by means of the Henry number ($H = 0.03$). Yang and Mao (2005) used the level-set method and presented two-dimensional numerical simulations of the mass transfer from a single drop rising in immiscible liquid. They considered the conjugate mass transfer with resistance in both drop and continuous phase ($Sc \approx 3000$) and an equilibrium distribution coefficient slightly different from unity ($H = 1.17$). Comprehensive two-dimensional investigations of the liquid-sided mass transfer from single bubbles and bubbles swarms with constant concentration in the bubbles have been performed by Koynov et al. (2005) and Koynov and Khinast (2006 and references therein) using a front-tracking method. The values of the bubble Reynolds number are $Re_B = 8$ and 68, respectively, while the Schmidt number is in the range 62–431 and homogeneous chemical reactions are allowed to occur within the continuous phase. In their method the species transport equation is solved on a finer grid than is used for the momentum equation. Radl et al. (2007) estimate that a three-dimensional direct numerical simulation with fully resolved boundary layers at realistic Schmidt and Peclet numbers is only possible with parallel machines using more than 10^9 grid points. Three-dimensional numerical simulations of the liquid-sided mass transfer from a single bubble with bubble Reynolds number in the range 5–130 and $Sc = 1$ are reported by Darmana et al. (2006). The authors use a front-tracking method and adopt for the species transport equation a grid that is three times finer than the one for the momentum equation. In all cases the concentration wake remains symmetrical and regular, while the different bubble shapes result in different flow fields around the bubble, influencing therefore the mass transport.

While the investigations mentioned above concern the mass transfer from spherical, ellipsoidal or irregular wobbling bubbles or drops, bubbles in millimetre or sub-millimetre channels are often elongated and the corresponding flow regime is known as Taylor flow or bubble train flow (Thulasidas et al., 1995, 1997). For Taylor flow there are up to now only very few numerical investigations of mass transfer reported in literature, which all rely on the assumption of axisymmetry and thus apply for circular capillaries only. In addition, they are based on rather restrictive assumptions such as a prescribed bubble shape consisting of a cylindrical body and hemispherical caps (Irandoust and Andersson, 1989; van Baten and

Krishna, 2004, 2005). Furthermore, at the gas–liquid interface a free slip condition is assumed and only the flow in the liquid phase is computed.

In contrast to these few numerical investigations, there exists a number of experimental studies on mass transfer in Taylor flow, both in single channels of circular (Horvath et al., 1973; Berčič and Pintar, 1997; Vandu et al., 2005; Tsoligkas et al., 2007b,c) and square or rectangular cross section (Vandu et al., 2005; Tsoligkas et al., 2007a; Yue et al., 2007) and in monoliths (Kreutzer et al., 2001, 2005). A main goal of these studies is to develop predictive correlations for the overall volumetric mass transfer coefficient $k_{ov}a$. The mass transfer from the bubble to the liquid is usually considered as the sum of two parts, namely: (i) mass transfer from the front and rear cap of the bubble to the liquid slug $k_{GL,cap}a_{cap}$ and (ii) mass transfer through the lateral surface of the bubble to the liquid film $k_{GL,film}a_{film}$ (Irandoust and Andersson, 1988; Kreutzer et al., 2001; Vandu et al., 2005). If a heterogeneous chemical reaction at the channel walls is considered two additional mass transfer processes have to be considered, namely: (iii) that from the liquid slug to the solid wall $k_{LS,slug}a_{LS,slug}$ and (iv) that from the liquid film to the wall $k_{LS,film}a_{LS,film}$. Then, contributions (i) and (iii) as well as (ii) and (iv) are in sequence and both are in parallel so that

$$k_{ov}a = \left(\frac{1}{k_{GL,cap}a_{GL,cap}} + \frac{1}{k_{LS,slug}a_{LS,slug}}\right)^{-1} + \left(\frac{1}{k_{GL,film}a_{GL,film}} + \frac{1}{k_{LS,film}a_{LS,film}}\right)^{-1} \quad (1)$$

Often, the contributions to the second bracket on the r.h.s. of Eq. (1) are not modelled separately but as one term (Irandoust and Andersson, 1988) and are denoted e.g. by Kreutzer et al. (2001) as $k_{GS}a_{GS}$. For pipes of larger diameter where the slug flow is turbulent, models are proposed in literature which divide the mass transfer near the wall in three (Ghosh and Cui, 1999) or four zones (Zheng and Che, 2007).

In Taylor flow, both the gas–liquid mass transfer from the bubble caps to the liquid slug and the liquid–solid mass transfer from the liquid slug to the channel walls are strongly influenced by the recirculation in the liquid slug (Irandoust and Andersson, 1989; Tsoligkas et al., 2007a). This recirculation occurs in co-current upward bubble train flow for long enough liquid slugs, $L_S/D_h > 1.5$, and for values of the capillary number less than about 0.47 (Thulasidas et al., 1997). The mass transfer from the bubble through the liquid film to the wall depends mainly on the thickness of the liquid film, which increases with increasing capillary number (Thulasidas et al., 1995). This is reflected by the model of Kreutzer et al. (2001) for mass transfer with chemical reaction at the walls. In this model, the mass transfer decreases with increasing gas and liquid velocities since these lead to an increased film thickness. The latter is associated with an increase of the diffusion length from the bubble toward the wall, which negatively affects the mass transfer. The different terms on the right-hand side of Eq. (1) thus depend on the capillary number, liquid slug length, bubble length and the liquid film saturation. Depending on these conditions, the term on the right-hand side of Eq. (1) that actually dominates mass transfer with or without chemical reaction may differ. This may be the reason why literature data are somewhat contradictory. E.g. Irandoust and Andersson (1989) report for mass transfer with heterogeneous chemical reaction that the major part of mass transfer occurs through the thin liquid film between the bubble and the wall, a result that is also found by van Baten and Krishna (2004, 2005). Berčič and Pintar (1997) report for a heterogeneous chemical reaction that the major part of the mass transfer occurs through the surfaces exposed to the liquid slug (since the liquid film is presumably saturated, see Vandu et al., 2005). Therefore, the length of the liquid slug is found to have a significant influence on mass transfer. Vandu et al. (2005) conclude in their study that the occurrence of the saturation in the liquid film in the experiments of Berčič and Pintar (1997) decreases the efficiency of the liquid film for mass transfer, while the liquid film is not saturated in the study performed by van Baten and Krishna (2004). Secondly, it is concluded that the volumetric mass transfer coefficient developed by Berčič and Pintar (1997) has a reduced applicability, since it does not involve the diameter of the capillary as is the case in other models (Irandoust and Andersson, 1988; Vandu et al., 2005). Nevertheless, it is interesting to mention that Heiszwolf et al. (2001) verified experimentally the correlation proposed by Berčič and Pintar (1997) and report that it can be applied to two-phase flows within monoliths. Vandu et al. (2005) proposed a criterion in terms of U_L, U_G, L_{slug} and t_{film} that identifies the regions of short and long contact times. For long contact times, saturation occurs within the liquid film and the volumetric mass transfer coefficient of Berčič and Pintar (1997) can be applied. For short contact times it is suggested that the volumetric mass transfer coefficient developed by van Baten and Krishna (2004) should be employed. Van Baten and Krishna (2005) report that the mass transfer in the wall–liquid film zone is significantly smaller than in the wall–liquid slug one. The reasons are the smaller wall–film area in comparison to the wall–liquid slug area and the occurrence of saturation within the liquid film. For estimation of the wall Sherwood number (Sh) a correlation in terms of a Graetz number (Gz) is proposed, where Gz depends on a variety of hydrodynamic parameters such as liquid slug length, gas holdup and liquid diffusivity (see Van Baten and Krishna, 2005). Interestingly, no significant influence of the bubble velocity on the relationship between Sh and Gz is found, while the influence of the gas content (obtained by varying the liquid slug length) is minimal.

A theoretical investigation of the mass transfer in bubble train flows with small bubbles in the liquid slug is reported by Elperin and Fominykh (1999). The model developed determines the transfer rate of mass from Taylor bubbles. It is reported that the mass flux is decreasing with increasing number of unit cells. The volumetric mass transfer coefficient is found directly proportional to the gas and liquid velocities, in agreement with Berčič and Pintar (1997). An interesting observation is that the contribution of the small bubbles within the liquid slug is considerable higher than the contribution of the Taylor bubble. In a later paper Elperin and Fominykh (2003) derived coefficients of mass transfer during chemical adsorption from a single Taylor bubble in the approximation of a thin concentration boundary layer in the liquid phase.

A controversial issue for Taylor flow in narrow channels is also the definition of an appropriate concentration difference which constitutes the driving force for mass transfer. In extended domains the mass transfer coefficient is usually based on the concentration in the bulk phase far away from the interface and the mean concentration in the disperse phase (e.g. Paschedag et al., 2005; Yang and Mao, 2005) or the concentration at the interface (e.g. Paschedag et al., 2002). Darmana et al. (2006) computed from their numerical results the mass transfer coefficient based on the concentration difference between two time steps. For mass transfer in confined non-circular mini-systems as they are investigated here, defining the concentration in the bulk phase far away from the bubble as well as at the interface is difficult, therefore a new formulation for the mass transfer coefficient is proposed.

In this paper we present investigations of mass transfer in Taylor flow by a new numerical method which conceptually overcomes many restrictions of previous studies on this topic. The numerical method is based on the VOF technique and is suitable for flows with mass transfer resistance in both phases and for a wide range of distribution coefficients. We present full three-dimensional transient simulations of mass transfer across deforming interfaces in upward bubble train flow within square and rectangular channels with a hydraulic diameter of 2 mm. We compare two cases with different

Henry number ($H = 0.03$ and 3), where the resistance to mass transfer is mainly in the continuous and in the disperse phase, respectively. Since our code is based on a uniform grid, we perform all simulations for an artificial species with Schmidt number of order one. This is to avoid the necessity to resolve thin concentration boundary layers by a grid, which is much finer than is already required by hydrodynamics. In a series of simulations we investigate the influence of the unit cell length, liquid slug length and channel aspect ratio on the effectiveness of mass transfer with and without a first-order homogeneous or heterogeneous chemical reaction.

The organization of the paper is as follows. In Section 2 we present the governing equations, describe the numerical method and perform a validation of the species conservation equation by several test problems. In Section 3 we present and discuss the numerical results for the mass transfer in bubble train flow in square and rectangular mini-channels. The conclusions are given in Section 4.

2. Numerical method

2.1. Hydrodynamic equations

The volume-averaged conservation equations for mass and momentum describing the flow of two immiscible incompressible fluids with constant material properties (density, viscosity, surface tension) and the transport equation for the liquid volumetric fraction as derived in Wörner et al. (2001) can be written in the following non-dimensional formulation:

$$\nabla \cdot \mathbf{v}_\mathrm{m} = 0 \tag{2}$$

$$\begin{aligned}\frac{\partial(\rho_\mathrm{m}\mathbf{v}_\mathrm{m})}{\partial\theta} + \nabla\cdot\rho_\mathrm{m}\mathbf{v}_\mathrm{m}\mathbf{v}_\mathrm{m} = &-\nabla P + \frac{1}{Re_\mathrm{ref}}\nabla\cdot\mu_\mathrm{m}(\nabla\mathbf{v}_\mathrm{m} + (\nabla\mathbf{v}_\mathrm{m})^\mathrm{T}) \\ &- (1-f)\frac{E\ddot{o}_\mathrm{ref}}{We_\mathrm{ref}}\hat{\mathbf{e}}_\mathrm{g} + Fr_\mathrm{ref}\hat{\mathbf{e}}_\mathrm{g} \\ &+ \frac{L_\mathrm{ref}}{L_\mathrm{axial}}Eu_\mathrm{ref}\hat{\mathbf{e}}_\mathrm{axial} + \frac{a_\mathrm{i}\kappa\hat{\mathbf{n}}_\mathrm{i}}{We_\mathrm{ref}}\end{aligned} \tag{3}$$

$$\frac{\partial f}{\partial\theta} + \nabla\cdot f\mathbf{v}_\mathrm{m} = 0 \tag{4}$$

In the above equations, ρ_m is the non-dimensional mixture density

$$\rho_\mathrm{m} \equiv \frac{f\rho_\mathrm{L} + (1-f)\rho_\mathrm{G}}{\rho_\mathrm{L}} \tag{5}$$

μ_m is the non-dimensional mixture viscosity

$$\mu_\mathrm{m} \equiv \frac{f\mu_\mathrm{L} + (1-f)\mu_\mathrm{G}}{\mu_\mathrm{L}} \tag{6}$$

and $\mathbf{v}_\mathrm{m}$ is the non-dimensional centre-of-mass velocity

$$\mathbf{v}_\mathrm{m} \equiv \frac{1}{U_\mathrm{ref}}\frac{f\rho_\mathrm{L}\mathbf{v}_\mathrm{L} + (1-f)\rho_\mathrm{G}\mathbf{v}_\mathrm{G}}{f\rho_\mathrm{L} + (1-f)\rho_\mathrm{G}} \tag{7}$$

Here, $\mathbf{v}_\mathrm{L} \equiv \overline{\mathbf{v}_1}^1$ and $\mathbf{v}_\mathrm{G} \equiv \overline{\mathbf{v}_2}^2$ are the intrinsic volume averaged phase velocities and $f \equiv \overline{X_1}^V$ is the volume averaged phase indicator function of the continuous phase (see Appendix A). Here, the averaging volume is taken to be equal to the volume of a mesh cell of our uniform grid. Therefore, f corresponds to the local liquid volumetric fraction in a mesh cell (which is 1 for liquid filled cells, 0 for gas filled cells and which may take any value between 0 and 1 for interface cells). The non-dimensional time θ is given by

$$\theta \equiv \frac{t}{t_\mathrm{ref}} = t\frac{U_\mathrm{ref}}{L_\mathrm{ref}} \tag{8}$$

where L_ref is a reference length scale and U_ref is a reference velocity scale.

Since the single-field Navier–Stokes equation (3) shall be applicable to a domain with periodic boundary conditions, the dimensionless "reduced" pressure P has been introduced, which is related to the dimensional physical pressure p via

$$P \equiv \frac{1}{\rho_\mathrm{L}U_\mathrm{ref}^2}\left(p + \frac{\bar{p}_0 - \bar{p}_{L_\mathrm{axial}}}{L_\mathrm{axial}}\hat{\mathbf{e}}_\mathrm{axial}\cdot\mathbf{x}\right) \tag{9}$$

Here, $\bar{p}_0$ is the plane-average of p over the cross section at $\mathbf{x} = 0$, while $\bar{p}_{L_\mathrm{axial}}$ is the plane-average across the cross section at $\mathbf{x} = L_\mathrm{axial}\hat{\mathbf{e}}_\mathrm{axial}$, with $\hat{\mathbf{e}}_\mathrm{axial}$ denoting the unit vector in axial direction. Due to this decomposition of the pressure term, the buoyancy term appears in the Navier–Stokes equation, Eq. (3), where $\hat{\mathbf{e}}_\mathrm{g}$ denotes the unit vector in the direction of gravity. The definitions of the non-dimensional numbers, based on the reference scales, appearing on the right-hand side of the Navier–Stokes Eq. (3) are

$$\begin{aligned}Re_\mathrm{ref} &\equiv \frac{\rho_\mathrm{L}L_\mathrm{ref}U_\mathrm{ref}}{\mu_\mathrm{L}}, \quad E\ddot{o}_\mathrm{ref} \equiv \frac{(\rho_\mathrm{L}-\rho_\mathrm{G})gL_\mathrm{ref}^2}{\sigma} \\ We_\mathrm{ref} &\equiv \frac{\rho_\mathrm{L}L_\mathrm{ref}U_\mathrm{ref}^2}{\sigma}, \quad Fr_\mathrm{ref} \equiv \frac{gL_\mathrm{ref}}{U_\mathrm{ref}^2}, \quad Eu_\mathrm{ref} \equiv \frac{\bar{p}_0 - \bar{p}_{L_\mathrm{axial}}}{\rho_\mathrm{L}U_\mathrm{ref}^2}\end{aligned} \tag{10}$$

The respective terms in Eq. (3) represent the viscous force ($\sim 1/Re_\mathrm{ref}$), the buoyancy force ($\sim E\ddot{o}_\mathrm{ref}/We_\mathrm{ref}$), the gravity force ($\sim Fr_\mathrm{ref}$), the force due to the external pressure gradient ($\sim Eu_\mathrm{ref}$) and the surface tension force ($\sim 1/We_\mathrm{ref}$).

The above equations have been implemented in our in-house computer code TURBIT-VOF (Sabisch et al., 2001; Ghidersa et al., 2004), which is based on a finite volume method and employs a regular Cartesian staggered grid. The solution of Eqs. (2) and (3) involves a projection method, where the resulting Poisson equation is solved by a conjugate gradient method. For time integration of the momentum equation (3) an explicit third-order Runge–Kutta scheme is employed. All spatial derivatives are approximated by second-order central difference schemes.

The volume fraction advection equation (4) is solved by means of a VOF method with interface reconstruction. The interface is locally approximated as a plane whose orientation and location within a mesh cell are determined by the EPIRA algorithm (exact plane interface reconstruction algorithm; Sabisch et al., 2001). In the un-split advection step of the VOF procedure the fluxes of liquid over the cell faces are computed in a geometrical manner.

2.2. Species transport equation for mass transfer

To allow the simulation of mass transfer phenomena, the non-dimensional volume-averaged species transport equation

$$\begin{aligned}&\frac{\partial c_\mathrm{m}}{\partial\theta} + \nabla\cdot c_\mathrm{m}\mathbf{v}_\mathrm{m} \\ &\quad = -\frac{1}{Re_\mathrm{ref}Sc_\mathrm{ref}}\left[\nabla\cdot\mathbf{j}_\mathrm{m} + (1-H)a_\mathrm{i}\overline{j_\mathrm{GL}}^{S_\mathrm{i}} + Da_\mathrm{ref}^\mathrm{hmg}f\frac{c_\mathrm{L}}{c_\mathrm{ref}}\right]\end{aligned} \tag{11}$$

as derived in Appendix A has been implemented in TURBIT-VOF (Onea, 2006) and is solved by the same explicit third-order Runge-Kutta time integration scheme that is also used for the momentum equation. Similar to the momentum equation, all spatial derivatives are approximated by second-order central differences. Eq. (11) can be solved for an arbitrary number of chemical species. The definition of the non-dimensional mixture concentration

$$c_\mathrm{m} \equiv \frac{fc_\mathrm{L} + (1-f)Hc_\mathrm{G}}{c_\mathrm{ref}} \tag{12}$$

Table 1
Computation of mixture diffusivity at cell face i+1/2 for a uniform grid.

	Patankar (1980)	Davidson and Rudman (2002)
Original formulation	$D_{\mathrm{m};i+1/2,j,k} = 2\left(\frac{1}{D_{\mathrm{m};i,j,k}} + \frac{1}{D_{\mathrm{m};i+1,j,k}}\right)^{-1}$	$D_{\mathrm{m};i+1/2,j,k} = \left(\frac{\lambda_{i+1/2,j,k}-0.5}{D_{\mathrm{m};i,j,k}} + \frac{1.5-\lambda_{i+1/2,j,k}}{D_{\mathrm{m};i+1,j,k}}\right)^{-1}$ $\lambda_{i+1/2,j,k} = \mathrm{Max}[\mathrm{Min}(f_{i,j,k} + f_{i+1,j,k}, 1.5), 0.5]$
Modification for present study	$D_{\mathrm{m};i+1/2,j,k} = 2\left(\frac{F_{i+1/2,j,k}}{D_{\mathrm{m};i,j,k}} + \frac{G_{i+1/2,j,k}}{D_{\mathrm{m};i+1,j,k}}\right)^{-1}$	$D_{\mathrm{m};i+1/2,j,k} = \left(F_{i+1/2,j,k}\frac{\lambda_{i+1/2,j,k}-0.5}{D_{\mathrm{m};i,j,k}} + G_{i+1/2,j,k}\frac{1.5-\lambda_{i+1/2,j,k}}{D_{\mathrm{m};i+1,j,k}}\right)^{-1}$
Condition for $F_{i,j,k}$	$F_{i+1/2,j,k} = \begin{cases} H & \text{for } (f_{i,j,k}=0) \wedge (0<f_{i+1,j,k}\leqslant 1) \\ 1 & \text{else} \end{cases}$	
Condition for $G_{i,j,k}$	$G_{i+1/2,j,k} = \begin{cases} H & \text{for } (0<f_{i,j,k}\leqslant 1) \wedge (f_{i+1,j,k}=0) \\ 1 & \text{else} \end{cases}$	

involves the Henry number, which expresses the ratio between the equilibrium concentrations on both sides of the interface

$$H \equiv \frac{c_{\mathrm{L}}^{\mathrm{eq}}}{c_{\mathrm{G}}^{\mathrm{eq}}} \tag{13}$$

In practice, the Henry number depends on temperature and pressure. In our simulations the flows are isothermal and have a small pressure gradient. Therefore, the Henry number is assumed to be constant.

Further quantities appearing in Eq. (11) are the non-dimensional mixture diffusive mass flux $\mathbf{j}_{\mathrm{m}}$ defined in Appendix A by Eq. (A.18), the reference Damköhler number for an optional first-order homogeneous chemical reaction in the liquid phase

$$Da_{\mathrm{ref}}^{\mathrm{hmg}} \equiv \frac{k_{\mathrm{hmg}} L_{\mathrm{ref}}^2}{D_{\mathrm{ref}}} \tag{14}$$

and the reference Schmidt number

$$Sc_{\mathrm{ref}} \equiv \frac{\mu_{\mathrm{L}}}{\rho_{\mathrm{L}} D_{\mathrm{ref}}} \tag{15}$$

Here, D_{ref} is the reference diffusivity, which is set equal to the diffusivity of the species in the liquid phase D_{L}. Alternative to a first-order homogeneous chemical reaction, a first-order heterogeneous chemical reaction at the channel walls may be considered. In the current implementation, the species conservation equation is without feedback on the Navier–Stokes equations, i.e. the mass transfer affects neither the velocity field nor the bubble size and shape.

In our approach we assume that the species concentrations on both sides of the interface are always in equilibrium. Then, by the inclusion of the Henry number H on the right-hand side of definition (12) it is ensured that c_{m} is continuous across the interface. By this procedure we avoid possible numerical difficulties which might appear when dealing with the physical concentrations c_{G} and c_{L}, which are discontinuous at the interface for $H \neq 1$. Such a transformation has recently become popular for mass transfer studies with the finite element method (Petera and Weatherley, 2001), the VOF method (Bothe et al., 2003) and the level-set method (Yang and Mao, 2005). Thus, while in the liquid c_{m} corresponds to $c_{\mathrm{L}}/c_{\mathrm{ref}}$, in the gas phase it corresponds to $Hc_{\mathrm{G}}/c_{\mathrm{ref}}$. There is, however, one significant drawback of this transformation. Namely, while the physical diffusive mass flux across the interface is continuous, this is not valid for the diffusive mass fluxes formulated in terms of the concentration c_{m}. As detailed in Appendix A, this gives in Eq. (11) rise to the term $(1-H)a_{\mathrm{i}}\overline{j_{\mathrm{GL}}}^{S_{\mathrm{i}}}$, which represents the volume average of the jump of the diffusive flux formulated in terms of c_{m}. Depending whether the Henry number is smaller or larger than unity, this term may act locally as source or sink term. It is non-zero in all mesh cells which contain a part of the interface, i.e. where the local volumetric interfacial area concentration a_{i} is positive. As a consequence of this term, the concentration c_{m} is not a conserved quantity for $H \neq 1$, even if there is no chemical reaction.

2.3. Computation of the diffusive mass flux

An important issue for the numerical solution of Eq. (11) is the computation of the diffusive terms, especially for mesh cells containing the interface. In our approach we do not compute the term $(1-H)a_{\mathrm{i}}\overline{j_{\mathrm{GL}}}^{S_{\mathrm{i}}}$ explicitly, but account for it by an appropriate computation of the finite difference representation of the mixture diffusive flux $\mathbf{j}_{\mathrm{m}}$ in interface mesh cells. The key idea is to modify the numerical computation of the mass flux at the interface in such a way that the continuity of the physical mass flux is ensured. As is shown in Appendix B, this can be done by an appropriate division of the diffusivity by H, which is performed for all mesh cells that are completely filled with gas and share a face with a mesh cell that contains the interface. Here, we shortly illustrate the computation of the diffusive flux in x-direction. The starting point is the cell centred mixture diffusivity which is, for a mesh cell (i,j,k), computed from the discrete values of the liquid volumetric fraction

$$D_{\mathrm{m};i,j,k} = \frac{f_{i,j,k} D_{\mathrm{L}} + (1-f_{i,j,k}) D_{\mathrm{G}}}{D_{\mathrm{ref}}} \tag{16}$$

Since in our code the diffusive term is discretized with a central difference scheme, the diffusivity D_{m} is needed at the position of the cell face i+1/2. For neighbouring mesh cells i and i+1 which contain only one phase, the cell face diffusivity simply corresponds to the diffusivity of that phase. For neighbouring mesh cells that contain different phases, the formulations proposed by Patankar (1980) and Davidson and Rudman (2002) for computation of the cell face diffusivity have been modified, see Appendix B, and implemented in TURBIT-VOF. The modifications are based on an appropriate inclusion of the Henry number H and are necessary since the original formulations are based on the assumptions that the concentration field is continuous at the interface and that the diffusive fluxes across the interface are equal. The formulation of Patankar (1980) considers the situation where the interface coincides with the common face of two neighbouring cells, while the formulation proposed by Davidson and Rudman (2002) allows both neighbouring cells to contain interfaces. The original and extended formulations valid for an uniform grid are presented in Table 1 together with the conditions for the cell face Henry numbers $F_{i+1/2,j,k}$ and $G_{i+1/2,j,k}$.

2.4. Validation of the species transport equation

The implementation of the species transport equation in TURBIT-VOF is validated against theoretical solutions of a number of different mass transfer problems, see Onea (2006). The validation of the diffusive term has been done by comparison to a one-dimensional time-dependant analytical solution given in Crank (1994) for two stagnant fluids separated by a plane interface. The initial dimensionless concentration in the liquid is zero, while in the gas phase it is unity. In Fig. 1(a) and (b) we show for the diffusivity ratio $D_{\mathrm{G}}/D_{\mathrm{L}} = 10$ and for a certain instant in time numerical solutions for $H = 0.5$ and 5, where for the latter case two different grids are

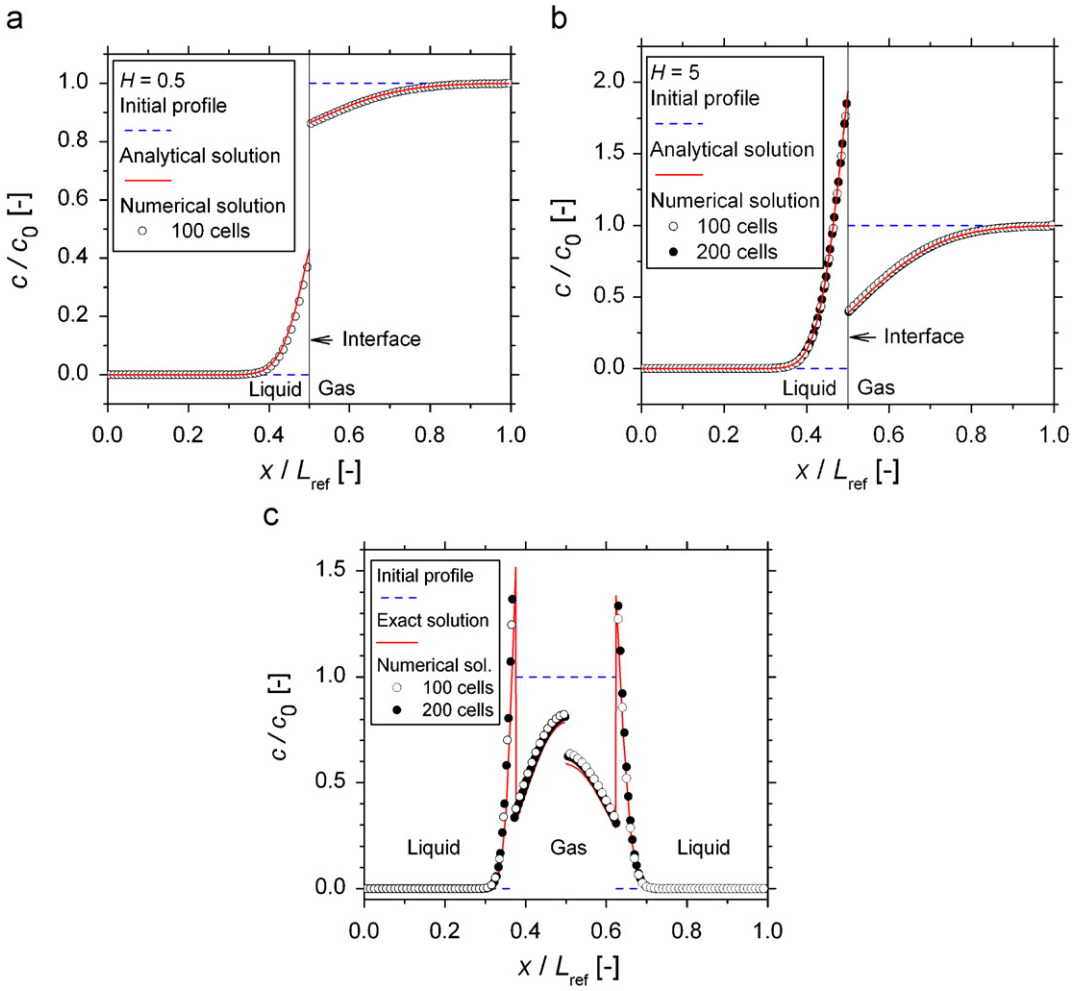

Fig. 1. Comparison between analytical and numerical solution for unsteady one-dimensional diffusive mass transfer across a plane interface (a and b) and a cylindrical interface (c). The diffusivity ratio is $D_G/D_L = 10$ and the solutions are displayed for a certain instant in time for $H = 0.5$ (a) and $H = 5$ (b) and (c). In figure (c) the left half corresponds to an earlier and the right half to a later instant in time.

considered. For all cases, the numerical results are in good agreement with the analytical solution. For these one-dimensional cases, no significant differences between the two modified formulations for the mixture diffusivity according to Table 1 have been found (Onea, 2006). For the remaining simulations presented in this study, the modified formulation of Davidson and Rudman (2002) has been employed. Comparisons for further values of H and D_G/D_L can be found in Onea (2006). Good agreement between the numerical and analytical solution is always obtained for $H < 1$. When the Henry number is much larger than unity, very sharp concentration gradients exist at the interface so that a good agreement between numerical and analytical solution is only obtained when this gradient is adequately resolved by a sufficiently fine grid.

To test the method for multi-dimensional problems, the diffusive mass transfer through a cylindrical interface is considered. Bothe et al. (2004) used a very fine grid to obtain numerically an "exact" solution, which is used for comparison. Similar to the one-dimensional case, good agreement with this "exact" solution has been obtained for all cases where the Henry number is smaller than unity, see Onea (2006). However, for values of H larger than 1 sharp concentration boundary layers develop, see Fig. 1(c) for $H = 5$. Fig. 1(c) shows that a grid refinement results in a better agreement with the exact solution. Nevertheless, the right half of Fig. 1(c) shows that even slight deficiencies in the resolution of the concentration gradient at the interface result in slight errors in the mass transfer rate across the interface, which accumulate over time and result here (for large values of D_G/D_L) in a grid-dependant overestimation of the concentration in the gas phase and an underestimation for the continuous phase. Thus, for cases with $H > 1$ very fine grids are required to adequately resolve these thin concentration boundary layers.

The implementation of the convective term and the sink term due to a homogeneous or heterogeneous chemical reaction has been verified by comparison to theoretical solutions reported by Apelblat (1980). There, the steady-state mass transfer with and without species consumption by a first-order homogeneous or heterogeneous chemical reaction in two-dimensional single phase flow over a horizontal wall is considered. The flow is unidirectional in x-direction with velocity $U_0 = 1$ m/s and Reynolds number $Re_{ref} = 10$. In the diffusion term, axial diffusion is neglected and only diffusion in the wall-normal direction y is considered. The diffusivity of the species is set to $D = 1\ m^2/s$. In the first case the species is consumed by a first-order homogeneous reaction in the entire domain and the wall is held at constant dimensionless concentration $c/c_{ref} = 1$. For the computations a uniform grid with 80×80 mesh cells is used and excellent agreement with the analytical solution is obtained, see Fig. 2(a). In the second case the species is consumed by a first-order heterogeneous reaction at the wall and both the inlet and the upper boundaries of the computational domain are held at constant

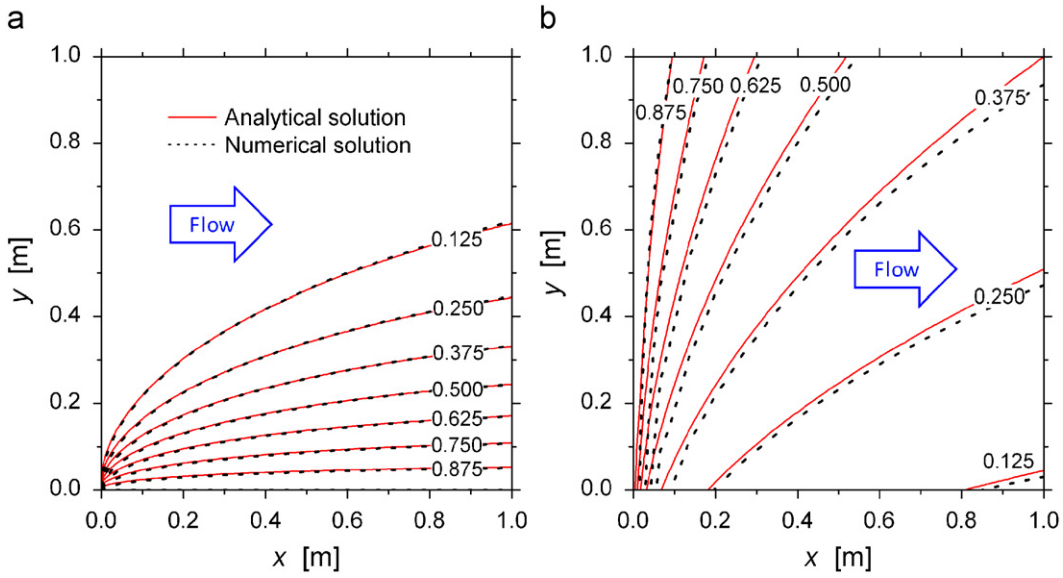

Fig. 2. Comparison between analytical and numerical solution for steady two-dimensional single phase flow and mass transfer with species consumption by a first-order chemical reaction. Isolines of the normalized concentration for: (a) homogeneous reaction ($k_{hmg} = 0.5/s^{-1}$, $Sc_{ref} = 1$, grid 80×80) and (b) heterogeneous reaction ($k_{htg} = 10\,m/s$, $Sc_{ref} = 0.1$, displayed grid 16×16).

concentration $c/c_{ref} = 1$. The non-dimensional size of the computational domain is 1×4, discretized by 16×64 uniform mesh cells. For the comparison with the analytical solution, only the lower part of the domain (16×16 mesh cells) is shown in Fig. 2(b). Though this grid is rather coarse, the agreement with the analytical solution is reasonable. Comparisons for further parameters are given in Onea (2006).

3. Results for mass transfer in bubble train flow

3.1. Numerical set-up and parameters

Flows in narrow devices often exhibit some regularity, i.e. flow structures that repeat themselves. From the numerical point of view this feature is often exploited by reducing the computational domain from the system size to the much smaller size of a unit cell. In our simulations, the unit cell consists of one bubble and one liquid slug, as displayed in Fig. 3. The coordinate system is defined so that the y-axis represents the stream-wise vertical direction with the gravity vector pointing in negative y-direction, while the x- and z-axis represent the wall-normal directions. The computational domain is a rectangular parallelepiped of size $L_x \times L_{uc} \times L_z$. The hydrodynamic boundary conditions for this domain are as follows: at the top and bottom periodic boundary conditions are employed while at the four side walls no-slip boundary conditions are applied. In this paper we consider the co-current vertical bubble train flow within square and rectangular vertical channels having a hydraulic diameter $d_h = 2\,mm$. In all simulations the value of the reference velocity is $U_{ref} = 0.0264\,m/s$ and $\hat{\mathbf{e}}_{axial} = -\hat{\mathbf{e}}_g = \hat{\mathbf{e}}_y$. Thus, the last two source terms on the r.h.s. of the momentum Eq. (3) can be combined as

$$Fr_{ref}\hat{\mathbf{e}}_g + \frac{L_{ref}}{L_{axial}} Eu_{ref}\hat{\mathbf{e}}_{axial} = \left(\frac{L_{ref}}{L_{axial}} Eu_{ref} - Fr_{ref}\right)\hat{\mathbf{e}}_y = \Pi\hat{\mathbf{e}}_y \qquad (17)$$

The simulations start without mass transfer from a state where an axisymmetric elongated bubble (similar to the one in Fig. 3) is placed in the centre of the domain and where both gas and liquid are initially at rest. The flow is driven by buoyancy and by the external pressure difference. After a short transient phase, the bubble adopts a steady shape and rises with constant velocity. The pressure difference $\bar{p}_0 - \bar{p}_{L_{axial}}$, respectively, Π according to Eq. (17), is adjusted

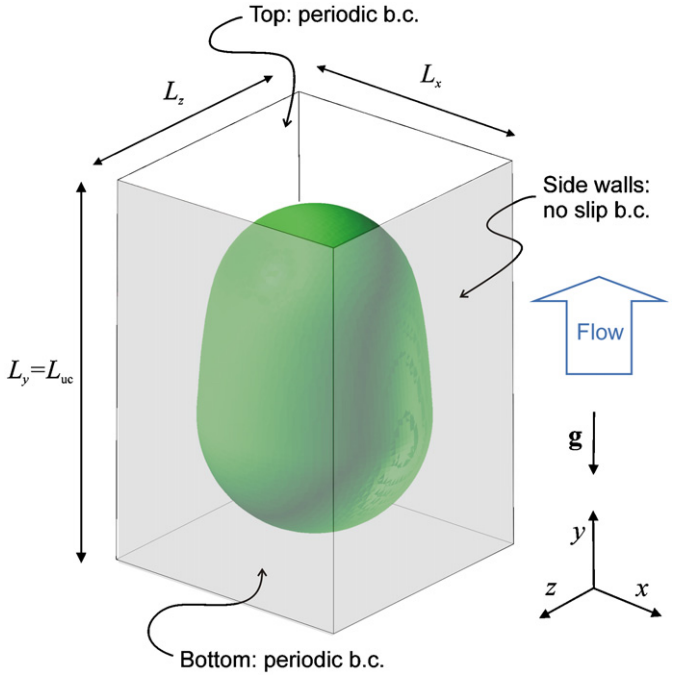

Fig. 3. Sketch of computational domain and coordinate system.

in such a manner so that the bubble velocity U_B is about the same for all simulations that shall be compared. This is to ensure that the capillary number

$$Ca \equiv \frac{\mu_L U_B}{\sigma} \qquad (18)$$

and the bubble Reynolds number

$$Re_B \equiv \frac{\rho_L d_h U_B}{\mu_L} \qquad (19)$$

are the same for these cases.

Table 2
Physical properties of the phases.

Fluid properties	Liquid	Gas
Density (kg/m^3)	957	11.7
Dynamic viscosity (Pa s)	0.048	1.824×10^{-4}
Species diffusivity (m^2/s)	62.24×10^{-6}	19.16×10^{-6}
Surface tension (N/m)	0.02218	

The physical properties of the two fluids are given in Table 2. The continuous liquid phase is silicone oil, while for the dispersed phase a gas with artificial properties is used. The gas density and viscosity are set 10 times higher than for air, in order to by-pass the increased CPU time of the Poisson solver for the real values. As shown by Wörner et al. (2007), this artificial increase of ρ_G and μ_G does not affect the shape and velocity of the bubble. The physical properties given in Table 2 result in the Morton number

$$Mo \equiv \frac{g(\rho_L-\rho_G)\mu_L^4}{\rho_L^2\sigma^3} = 49.26\times10^{-4} \tag{20}$$

When a fully developed flow has been reached, the simulation of mass transfer is launched. For all cases, the initial concentration in the gas phase is set to $c_G = c_{ref} = 1\,\mathrm{mol/m^3}$, which corresponds to the dimensionless concentration $c_m = H$ within the bubble. The initial concentration in the continuous liquid phase is zero. The boundary conditions for the species Eq. (11) are as follows. At the top and bottom of the unit cell again periodic boundary conditions are used, which are justified by the short periods of time that are simulated. At the four channel side walls Neumann boundary conditions are applied. These are either homogeneous (i.e. zero flux for mass transfer without or with homogeneous chemical reaction) or heterogeneous (i.e. non-zero flux for mass transfer with a first-order heterogeneous chemical reaction).

The diffusivities of the species in both phases are given in Table 2. The gas diffusivity corresponds to the diffusivity of oxygen in air, while the diffusivity in the liquid has been deliberately chosen approximately 30 000 times higher than the diffusivity of oxygen in water so that $D_L/D_G \approx 3.25$. In all present simulations the Schmidt number for the liquid phase Sc_L is about 0.8. For such a Schmidt number of order unity the thickness of the concentration boundary layer is about the same as that of the viscous boundary layer. Thus, one could expect that for the mass transfer study there should be no need to use a finer grid than is already required from pure hydrodynamic aspects. Hasegawa and Kasagi (2006) discuss the grid requirements for turbulent mass transfer at a flat free surface. They estimate that the number of grid points is proportional to $Sc^{3/2}$. Thus, realistic Schmidt numbers of order 1000 require grids that are much finer than can be afforded here. Beside the grid requirement aspect for high Schmidt number flows, there is also a second aspect for the artificial increase of the species diffusivity in the liquid phase. Due to the increase of D_L, diffusive processes in the liquid phase are much faster and the CPU time for the transient simulations can be drastically reduced. Only due to this, the present transient three-dimensional numerical simulations become feasible.

In this paper, two different values for H are considered, namely $H = 0.03$ and 3. The value $H = 0.03$ is representative for mass transfer of oxygen in air/water flow and was already used in the numerical simulations of Bothe et al. (2004). The value $H = 3$ is representative for methyl chloride (CH_3Cl) in water (Sander, 1999).

3.2. Influence of the unit cell length on mass transfer

The parameters for all present simulations are listed in Table 3. In our first series of simulations we consider a square channel with $L_x = L_z = L_{ref} = 2\,\mathrm{mm}$. To investigate the influence of the length of the unit cell on mass transfer, three values of L_{uc} are considered, namely $L_{uc} = 2\,\mathrm{mm}$ (case A), 2.75 mm (case B) and 3.5 mm (case C). In all three cases the gas content within the computational domain is $\varepsilon \approx 33\%$ and the value of Ca is about 0.208 and that of Re_B is about 3.84. For the influence of the unit cell length on the hydrodynamics of bubble train flow we refer to Wörner et al. (2007). In this paper also a grid refinement study is performed, which shows that a uniform grid with 48×48 mesh cells per channel cross-section is sufficiently fine. The time step width used is $\Delta t/t_{ref} = 2.5\times10^{-5}$ for all cases with exception of case G where it is 2.0×10^{-5}.

Fig. 4 shows the computed steady bubble shape in a vertical midplane for cases A, B and C. Since the gas hold-up is fixed to about 33%, an increase of L_{uc} does not only result in an increase of the length of the bubble but also of that of the liquid slug. In the left half of Fig. 4(a)–(c) we display the streamlines in the liquid phase and in the right half the velocity field, all evaluated in a frame of reference moving with the bubble. One can observe in all cases a toroidal vortex in the bubble and—for case B and C—one in the liquid slug. In case A, the liquid slug is too short for a clear vortex to be formed. Though the bubble velocity is similar in all cases, one can observe that the intensity of the toroidal vortex in the bubble increases with increasing length of the bubble and the unit cell.

For validation of the flow hydrodynamics, we compared the simulation results for the non-dimensional bubble diameter d_B/d_h, the relative velocity $(U_B - J)/U_B$ and the ratio U_B/J with experimental data of Thulasidas et al. (1995). Here, $J \equiv \varepsilon U_B + (1-\varepsilon)U_L$ is the total superficial velocity. For all three quantities reasonable agreement is obtained not only for the present simulations (see Onea et al., 2007) but also for simulations performed in a previous study (Wörner et al., 2007). The performance of our code for bubble train flow in a narrow channel has also been compared with that of three commercial CFD codes (Özkan et al., 2007). It was found that the results of TURBIT-VOF and FLUENT, which have a state of the art VOF method based on piecewise linear interface calculation, are in good agreement and are clearly superior to codes as CFX and STAR-CD, which use no interface reconstruction to solve the volume fraction advection equation but use difference schemes instead.

Within this study, the mass transfer is mainly evaluated in terms of the normalized mean species concentration in the gas phase, $\langle c_G(t)\rangle_{VG}/c_G^0$. Here, c_G^0 is the initial concentration in the bubble and the symbol $\langle\cdot\rangle_{VG}$ denotes the volume average over the gas phase. For our grid of uniform mesh size, the mean species concentration in the bubble is for any instant in time computed as

$$\langle c_G(t = n\Delta t)\rangle_{VG} = \frac{1}{H}\sum_{i,j,k} c^n_{m;i,j,k}(1 - f^n_{i,j,k}) \tag{21}$$

While initially the value of $\langle c_G(t)\rangle_{VG}/c_G^0$ is unity, it asymptotically approaches a smaller value for long times. Since we use periodic boundary conditions not only for the hydrodynamics but also for the species transport equation, this asymptotic equilibrium value can be computed from the following species mass balance

$$c_G^0 V_G = c_G^{eq} V_G + c_L^{eq} V_L, \tag{22}$$

where V_G and V_L are the volume of the bubble and of the liquid within the unit cell. Considering the definition of the Henry number in Eq. (13) and that of the gas hold-up $\varepsilon \equiv V_G/(V_G + V_L)$, we obtain from Eq. (22) the result

$$\frac{c_G^{eq}}{c_G^0} = \frac{1}{H}\frac{c_L^{eq}}{c_G^0} = \frac{1}{1 + H(1/\varepsilon - 1)} \tag{23}$$

For $H = 0.03$ and $\varepsilon = 0.33$, the normalized mean concentration at equilibrium is $c_G^{eq}/c_G^0 = 0.943$ for the gas phase and is $c_L^{eq}/c_{ref} = 0.028$ for the liquid phase. In Fig. 5(a) it can be seen that for increasing

Table 3
Overview of simulations for mass transfer in bubble train flow.

Case	$L_{uc} = L_y$ (mm)	$L_z = L_{ref}$ (mm)	L_x/L_z (dimensionless)	Grid	ε (%)	Π (dimensionless)	U_B (m/s)	U_L (m/s)	a (m^2/m^3)	U_B/J (dimensionless)	Z (dimensionless)	d_B/d_h (dimensionless)
Variation of unit cell length ($H = 0.03$ and $H = 3$; $Da_{hmg} = 1272.5$; $Da_{htg} = 42.4$)												
A	2	2	1	48×48×48	33.0	27.03	0.0964	0.0319	1166	1.812	0.448	0.822
Ar	2	2	1	80×80×80	33.0	27.53	0.0968	0.0321	1166	1.809	0.447	0.811
B	2.75	2	1	48×66×48	33.3	26.23	0.0964	0.0345	1074	1.755	0.43	0.846
C	3.5	2	1	48×84×48	33.1	23.80	0.0969	0.0349	1007	1.749	0.428	0.858
										L_B (mm)	L_{LS} (mm)	d_B/d_h (dimensionless)
Variation of liquid slug length ($H = 0.03$; $Da_{hmg} = 12.7$ and 1272.5; $Da_{htg} = 0.0042$ and 42.4)												
D	2.75	2	1	48×66×48	33.0	27.03	0.099	0.035	1074	2.27	0.48	0.847
E	3.33	2	1	48×80×48	24.8	35.82	0.100	0.042	921	2.16	1.173	0.838
										L_B (mm)	L_{LS} (mm)	
Variation of channel aspect ratio ($H = 0.03$; $Da_{hmg} = 1272.5$; $Da_{htg} = 42.4$)												
F	2.5	2	1	48×60×48	33.0	27.03	0.0956	0.034	1094	2.1	0.4	
G	2.475	1.8	1.25	60×66×48	33.0	24.00	0.0956	0.033	1082	2.115	0.36	
H	2.4375	1.625	1.6	64×60×40	33.1	21.24	0.0956	0.03	1099	2.215	0.22	

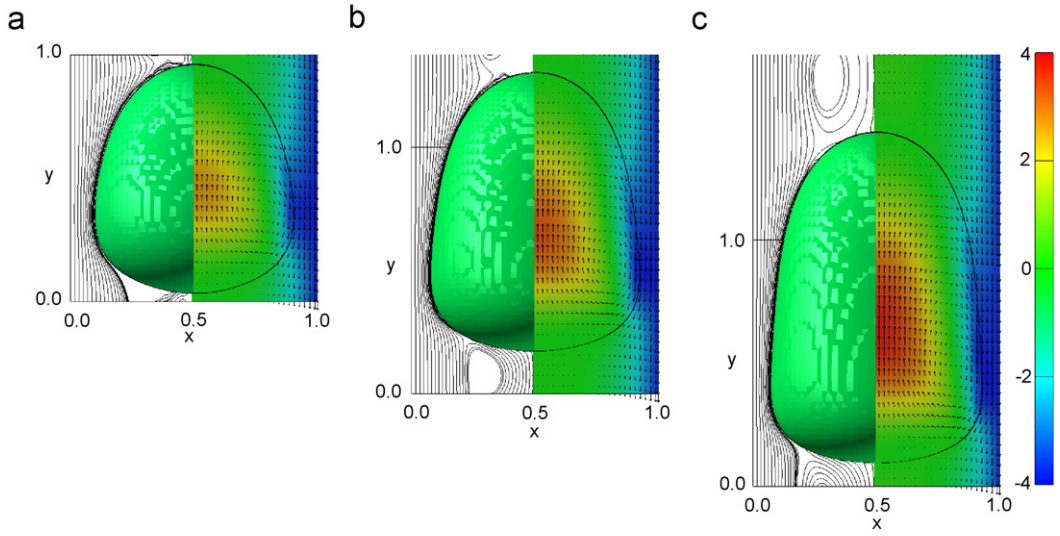

Fig. 4. Visualization of stream lines (left half), velocity vectors (right half) and non-dimensional vertical velocity (colour code in right half) in moving frame of reference for plane $z = 1$ mm for: (a) case A, (b) case B and (c) case C.

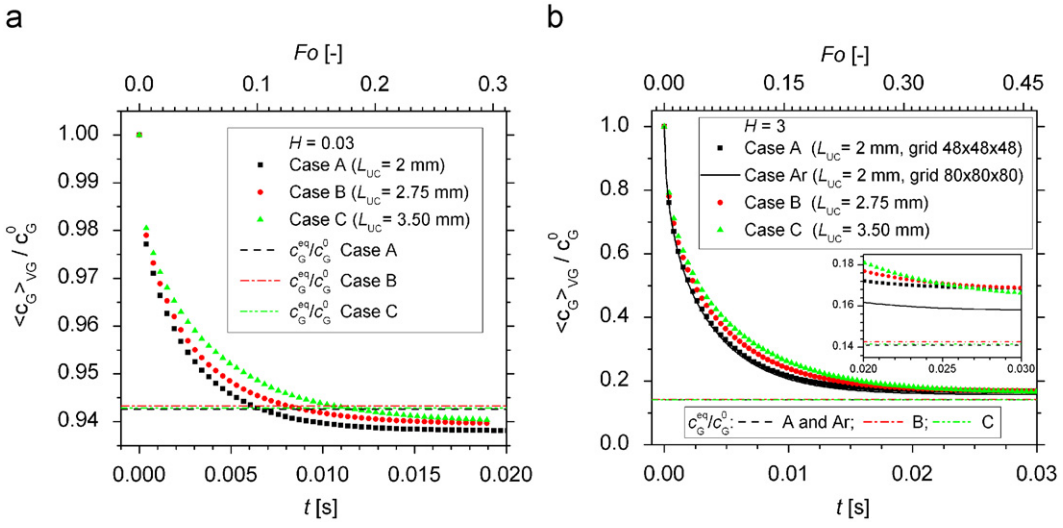

Fig. 5. Influence of unit cell length on mass transfer in terms of normalized mean gas concentration for: (a) $H = 0.03$ and (b) $H = 3$.

time, respectively, Fourier number $Fo \equiv D_L t/d_h^2$, the normalized mean concentration in the gas phase $\langle c_G(t)\rangle_{VG}/c_G^0$ approaches constant values for all three cases A–C. However, these values are slightly but distinctly smaller than the respective equilibrium values c_G^{eq}/c_G^0 computed from Eq. (23), which are shown in Fig. 5(a) as horizontal lines. The time evolutions of $\langle c_G(t)\rangle_{VG}/c_G^0$ for cases A, B and C with $H = 3$ are shown in Fig. 5(b). For all three cases, the asymptotic value of $\langle c_G(t)\rangle_{VG}/c_G^0$ is now clearly larger than the equilibrium value, which is $c_G^{eq}/c_G^0 = 0.141$ for the gas phase (and $c_L^{eq}/c_G^0 = 0.423$ for the liquid phase). To investigate the influence of grid resolution, an additional simulation on a refined grid with 80×80×80 mesh cells is performed for case A with $H = 3$ (case Ar). It can be observed from Fig. 5(b) that the deviation of $\langle c_G(t)\rangle_{VG}/c_G^0$ from c_G^{eq}/c_G^0 reduces from about 19% for the coarse mesh (case A with 48×48×48 mesh cells) to about 12% for the refined mesh. This improvement can be attributed to the fact that the concentration boundary layers on both sides of the interface are better resolved. However, as was already observed in the test case for the cylindrical bubble of Section 2.4, very fine grids are required for cases with $H > 1$. Obviously, the 80×80×80 grid of case Ar with $H = 3$ is not sufficiently fine though the Schmidt number is only 0.8.

While the concentration c_m is not a conserved quantity, the results presented in Fig. 5 can nevertheless be used to estimate the numerical error in conservation of molar mass. For any instant in time the molar mass within the computational domain is given by

$$N(t) = \langle c_G(t)\rangle_{VG}\varepsilon V_{uc} + \langle c_L(t)\rangle_{VL}(1-\varepsilon)V_{uc} \tag{24}$$

so that the relative error $(N(t)–N_0)/N_0$ can be computed from the evaluated values for $\langle c_G(t)\rangle_{VG}$ and $\langle c_L(t)\rangle_{VL}$. While in Fig. 5(a) the results for case A are only displayed till $t = 0.02$ s, this simulation has nevertheless been continued till $t = 0.057$ s. From $t = 0.02$ to 0.057 s the value of $\langle c_G(t)\rangle_{VG}/c_G^0$ decreases very slightly from 0.93873 to 0.93796. During the 30 000 time steps of this simulation the relative error in molar mass is −0.5%. For $H = 3$ and cases A and Ar, this error is about 19% and 12%, respectively. Thus, for all these cases the relative error in molar mass conservation takes the same value as the relative deviation of the terminal normalized mean gas concentration from the theoretical equilibrium value. We thus note that our present first results for mass transfer in bubble train flow for case $H = 3$ are not grid-independent and thus must be considered qualitative in nature. Such qualitative computations are, however, useful to explore the potential of the new method, while quantitative grid-independent computations on much finer grids will be a next step to be undertaken in future investigations. A suitable procedure for such computations will be to solve the species transport equation on a finer grid than is used for the momentum equation, an approach that is already used by Koynov et al. (2005) and Darmana et al. (2006).

The results presented in Fig. 5(a) and (b) show that short unit cell systems reach the equilibrium state faster than longer unit cell configurations, both for $H = 0.03$ and 3. To investigate the reason for this we display, for case C only, in Fig. 6 visualizations of the concentration field in different planes and associated local concentration profiles, both for $H = 0.03$ (Fig. 6a and c) and $H = 3$ (Fig. 6b and d). In Fig. 6(a) and (b), a high density of isolines close to the interface indicates high concentration gradients and thus high resistance to mass transfer. Within one phase, a high density of isolines indicates locally high relative mass transfer rates, whereas a low density of isolines indicates small concentration gradients and locally small mass transfer rates. For $H = 0.03$ the equilibrium concentration in the bubble is higher than in the liquid and the mass transfer at the interface is from high concentration to low concentration. Fig. 6(a) and (c) show, that the concentration in the bubble is rather uniform and the main resistance to mass transfer is on the liquid side of the interface. In the liquid phase high local mass transfer rates are found at the bubble front and rear, whereas at the lateral sides of the bubble the instantaneous concentration in the liquid film is rather uniform. It takes values that are larger than the liquid concentration at terminal equilibrium, while the concentration in the thicker liquid film in the corner of the channel is much lower. Longer unit cell configurations exhibit a larger contact area between the bubble lateral sides and the channel walls than short unit cell systems. The liquid film developed in this contact area provides a buffer zone in which species is rapidly accumulating due to short diffusion lengths and large exposure time. Therefore, the concentration in the liquid film rapidly reaches a level that is in equilibrium with the concentration inside the bubble. This decreases the efficiency of the liquid film for further mass transfer. Thus, for subsequent times the mass transfer occurs to the major part through the front and rear of the bubble, where due to the recirculation in the liquid slug the liquid is continuously refreshed, while the lateral sides of the bubble contribute only to a minor part. This is the reason why, for a given void fraction within the unit cell, short unit cells are more efficient for mass transfer than long unit cells, as displayed in Fig. 5(a).

For $H = 3$ the equilibrium concentration in the bubble is smaller than in the liquid and the mass transfer at the interface is from low concentration to high concentration. Fig. 6(b) and (d) show that for this case the main resistance to mass transfer is on the gas side of the interface. In the liquid, the concentration in the film and corner region is much higher than in the liquid slug and is higher than the terminal liquid equilibrium concentration, similar to the case with $H = 0.03$. For this reason also for $H = 3$ short unit cells are more efficient for mass transfer, as indicated by Fig. 5(b).

The degree of saturation of the liquid film can be quantified by the time of exposure t_{exp} (or contact time) of the liquid film and the corresponding Fourier number. Commonly, t_{exp} is computed as the ratio between the length of the liquid film (or the length of the bubble) and the bubble velocity, i.e. $t_{exp} = L_{LF}/U_B$. The length of the liquid film is evaluated here from Fig. 4 as the length over which the diameter of the bubble is larger than $0.8d_h$. The values are given in Table 4 and compared to the estimation $L_{LF} \approx L_{uc}\varepsilon$ proposed by Vandu et al. (2005). It is found that the latter formula gives reasonable values for case B and C but not for the very short unit cell of case A. Based on the exposure time a Fourier number can be defined

$$Fo_{exp} \equiv \frac{D_L t_{exp}}{\delta_{LF}^2} \tag{25}$$

In this equation, the lateral thickness of the liquid film is computed from the bubble diameter by relation $\delta_{LF} = (d_h - d_B)/2$. The exposure time is denoted as short if $Fo_{exp} < 1$ and as long if $Fo_{exp} > 1$ (Toor and Marchello, 1958). For long exposure times, respectively, large values of Fo_{exp}, saturation occurs in the liquid film leading to inefficient local mass transfer (Pohorecki et al., 2008). As shown in Table 4, in our simulations the Fourier number is clearly larger than unity.

For the definition of the overall mass transfer coefficient we propose a formulation where the driving force for mass transfer is constituted by the time-dependant mean concentrations of both phases within the unit cell. In this way we avoid the employment of constant bulk concentrations, since these seem not to be realistic for mass transfer of a dilute species within a confined narrow channel. As shown in Appendix C, for the present problem the following formulation for the overall mass transfer coefficient can be derived

$$k_{ov}^G(t) = \frac{-\frac{1}{a_i}\frac{d}{dt}\frac{\langle c_G(t)\rangle_{VG}}{c_G^0}}{\frac{\langle c_G(t)\rangle_{VG}}{c_G^0}\left(\frac{1}{\varepsilon} + \frac{1}{H(1-\varepsilon)}\right) - \frac{1}{H(1-\varepsilon)}} \tag{26}$$

This mass transfer coefficient can be computed from the time history of the normalized mean concentration in the gas phase, displayed in

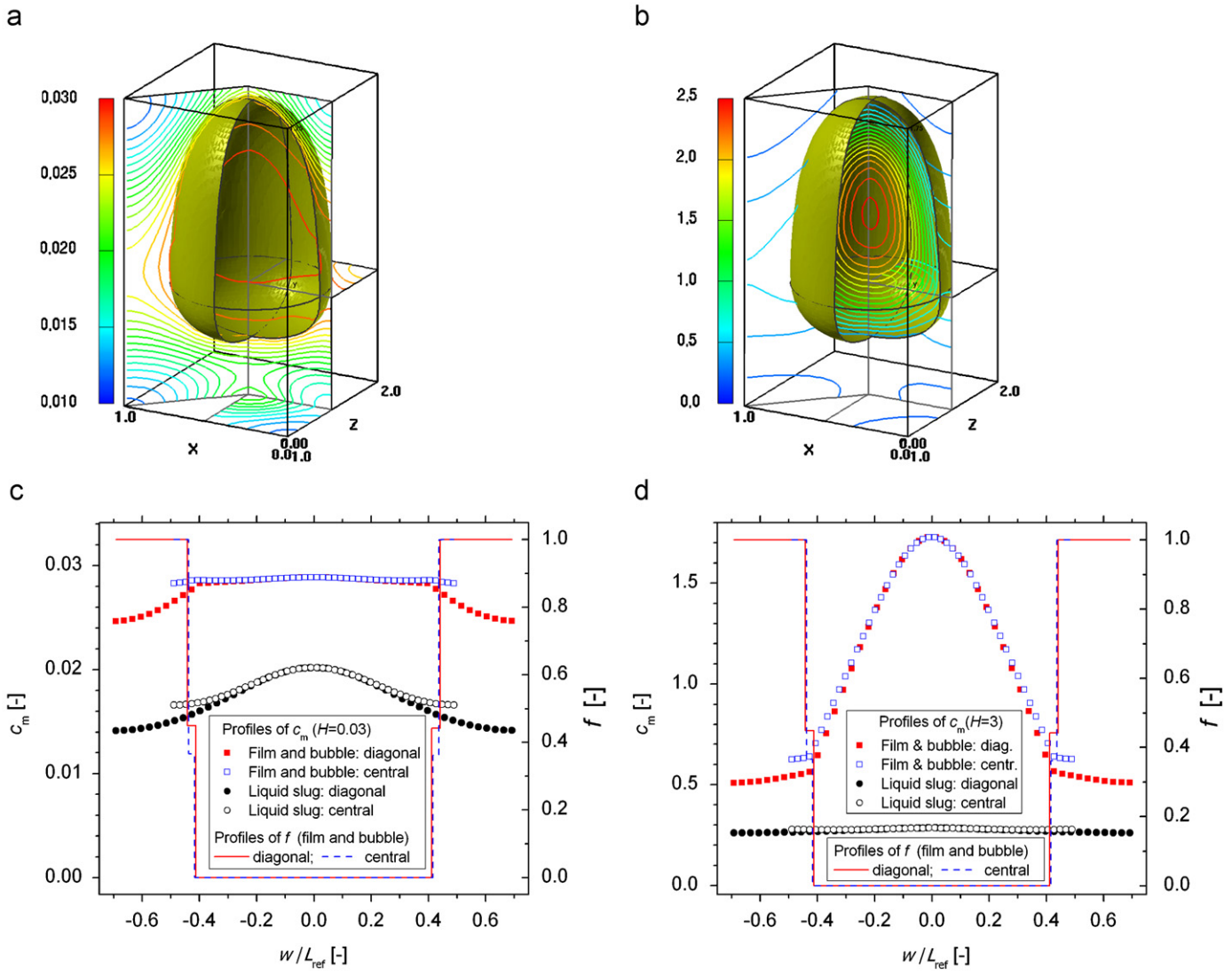

Fig. 6. Isolines of the transformed continuous concentration field c_m for case C at $t = 0.005$ s in different vertical and horizontal planes for $H = 0.03$ (a) and $H = 3$ (b). In both figures the range in the colour legend is resolved by 20 isolines. Figures (c) and (d) show corresponding profiles of c_m at representative axial positions in the film and bubble region ($y/L_{ref} = 0.37$) and in the middle of the liquid slug ($y/L_{ref} = 0.08$), both in the channel centre ($z/L_{ref} = 0.49$, $-0.5 \leqslant w/L_{ref} \leqslant 0.5$, $w = x - L_{ref}/2$) and along its diagonal ($-0.5\sqrt{2} \leqslant w/L_{ref} \leqslant 0.5\sqrt{2}$, $w = (x - L_{ref}/2)\sqrt{2}$) for $H = 0.03$ and $H = 3$, respectively.

Table 4
Lateral thickness of the liquid film, liquid film length, time of exposure and corresponding Fourier number.

Case	A	B	C
δ_{LF} (mm)	0.18	0.19	0.14
L_{LF} (mm)	0.42	0.80	1.18
εL_{uc} (mm)	0.66	0.92	1.16
$t_{exp} = L_{LF}/U_B$ (ms)	4.36	8.30	12.18
Fo_{exp} (dimensionless)	8.37	21.78	38.67

Fig. 5. The mass transfer coefficient $k_{ov}^{G}(t)$ is displayed in Fig. 7 for cases A, B and C, both for $H = 0.03$ and 3. We first discuss the results for $H = 3$. The comparison of case A and Ar (refined grid) shows that the mass transfer coefficient slightly varies with grid resolution. The reason is that the denominator of Eq. (26) is a measure for the deviation from the theoretical concentration at equilibrium. As shown in the inset graphics of Fig. 5(b) and discussed above, the agreement with the theoretical equilibrium concentration is much better for case Ar than for case A. This results in a slightly higher value of $k_{ov}^{G}(t)$ though qualitatively the curves for case A and Ar are similar. The comparison of cases A, B and C shows that for $H = 3$ the mass transfer coefficient is almost independent from the length of the unit cell, especially for $t < 10$ ms. This indicates that for $H = 3$ the better mass transfer efficiency of short unit cells in Fig. 5(b) is due to the slightly higher values of the interfacial area concentration, see Table 3.

For $H = 0.03$ Eq. (26) gives reasonable values for $k_{ov}^{G}(t)$ only for $t < 5$ ms. For larger values of t the denominator of Eq. (26) approaches zero and then becomes negative, resulting in an unphysical singularity of $k_{ov}^{G}(t)$ and negative values for large times. The reason is that for $t \approx 6$–12 ms the curves for $\langle c_G(t)\rangle_{VG}/c_G^0$ in Fig. 5(a) fall below the theoretical equilibrium values. The inset graphics in Fig. 7 shows, however, that for $H = 0.03$ the mass transfer coefficient is somewhat higher for the shorter unit cells. Therefore, for $H = 0.03$ the better mass transfer efficiency of short unit cells which can be seen in Fig. 5(a) is a results of both, a higher value of the interfacial area concentration and a higher value of the mass transfer coefficient of short

unit cells. This finding is in qualitative agreement with results of van Baten and Krishna (2004) for mass transfer in Taylor flow within circular channels, who reported that the volumetric mass transfer coefficient is inversely proportional to the unit cell length. It should, however, be mentioned that in their numerical study the liquid film between the bubble lateral side and the walls is not saturated.

We now discuss the simulation results for mass transfer accompanied by a first-order homogeneous chemical reaction. The reaction constant is set to $k_{\mathrm{hmg}} = 19\,800\,\mathrm{s}^{-1}$. This results in a Damköhler number

$$Da_{\mathrm{hmg}} \equiv \frac{k_{\mathrm{hmg}} d_{\mathrm{h}}^2}{D_{\mathrm{L}}} = 1272.5 \tag{27}$$

that is large, suggesting that the chemical reaction has a fast character. For all simulations in this paper where the species is consumed by a homogeneous chemical reaction, the reaction occurs only if the local solute concentration in the liquid exceeds the artificially set limit of 1.5% of the reference concentration. This is in order to obtain a certain concentration level in the liquid phase by physical mass transfer before the reaction can start. The results for the homogeneous reaction for cases A, B and C are shown in Fig. 8(a). Both, for $H = 0.03$ and 3 it is found that short unit cells systems transfer more solute per time into the continuous phase than long unit cell systems. Thus, the amount of species available for reaction till a certain instant in time is also larger for short unit cells. Fig. 8(a) shows that the mass transfer across the interface is much faster for $H = 3$ than for $H = 0.03$. A visualization of the instantaneous concentration field (not shown here) indicates that the concentration in the liquid is uniform with a value of $c_{\mathrm{L}}/c_{\mathrm{ref}} = 0.015$ at which the reaction occurs. This is attributable to the large liquid diffusivity and to the fast character of the chemical reaction. The mass transfer occurs to the major part through the bottom of the bubble where the interfacial area is largest.

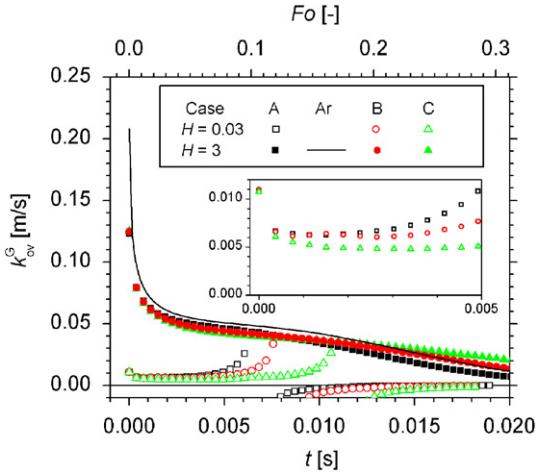

Fig. 7. Mass transfer coefficient for cases A, B and C determined with Eq. (26) for $H = 0.03$ and 3.

For mass transfer with species consumption by a first-order heterogeneous chemical reaction the reaction constant is set to $k_{\mathrm{htg}} = 1.32\,\mathrm{m/s}$. This results in a Damköhler number

$$Da_{\mathrm{htg}} \equiv \frac{k_{\mathrm{htg}} d_{\mathrm{h}}}{D_{\mathrm{L}}} = 42.4 \tag{28}$$

which is also large, signifying that the reaction is fast, too. The results are displayed in Fig. 8(b) in terms of the normalized mean gas concentration. For $H = 3$ the trend is similar to that for the homogeneous reaction. Namely, short unit cells are slightly more efficient for mass transfer. A detailed comparison of the curves displayed in Fig. 8(a) and (b) for $H = 3$ shows that for each case A–C the mass transfer for the homogeneous reaction is only slightly faster than for the heterogeneous reaction. Furthermore, the data for case A with heterogeneous reaction are similar to those for case B with heterogeneous reaction. These results suggest that for this case the resistance to mass transfer from liquid-to-solid is much smaller than that from gas-to-liquid. However, for $H = 0.03$ the situation is different. Here, for each case A–C mass transfer with homogeneous reaction is clearly more efficient than mass transfer with heterogeneous reaction. However, the slopes of the curves suggest that there might be a crossover for $t > 0.03$ s though this conjecture cannot be proved since the simulations have not been continued so far.

An interesting result in Fig. 8(b) is that for the heterogeneous chemical reaction with $H = 0.03$ the influence of the unit cell length is opposite to all other cases considered up to now. Here the mass transfer for the shortest unit cell (case A) is slightly less efficient than for the two longer unit cells (case B and C), whose results are almost identical. To investigate the reason for this we consider in Fig. 9 visualizations of instantaneous concentration isolines in different planes for case C. We see from Fig. 9(b) that for $H = 3$ the concentration in the liquid is almost uniform while there is a large resistance to mass transfer inside the bubble. The influence of the unit cell length is therefore similar to the cases without chemical

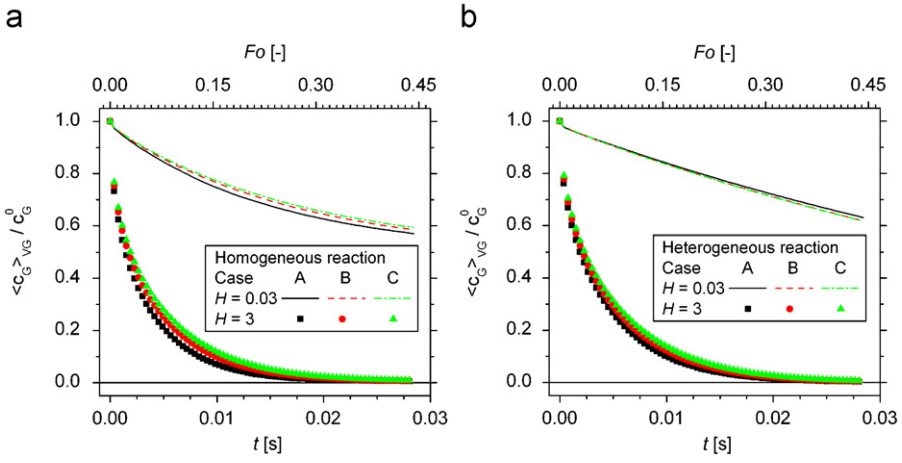

Fig. 8. Influence of unit cell length on mass transfer with species consumption by: (a) a first-order homogeneous reaction and (b) a first-order heterogeneous reaction.

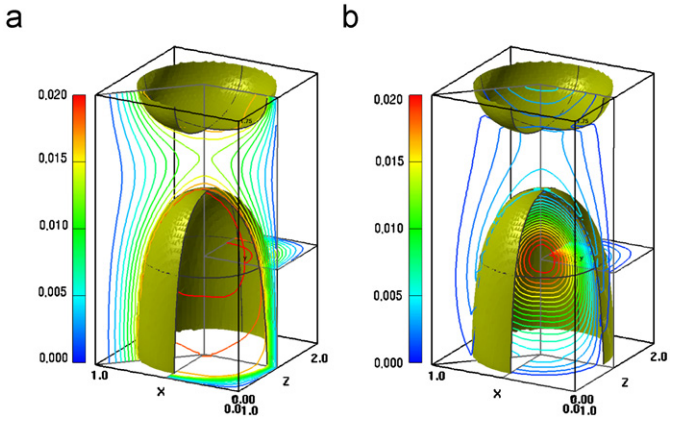

Fig. 9. Isolines of continuous concentration field c_m for case C in case of mass transfer with heterogeneous reaction at $t = 0.028$ s in different vertical and horizontal planes for $H = 0.03$ (a) and $H = 3$ (b). The range in the colour legend is resolved by 12 isolines for figure (a) and by 20 isolines for figure (b).

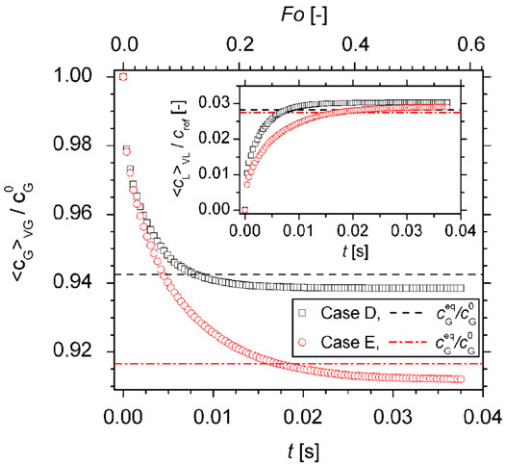

Fig. 10. Normalized mean concentration of gas and liquid (inset graphics) for short (case D) and long (case E) liquid slug. The horizontal lines denote the theoretical concentration at equilibrium in gas and liquid for both cases ($H = 0.03$).

reaction and with homogeneous reaction, where mass transfer is found to be more efficient for short unit cells. Fig. 9(a) shows that for $H = 0.03$ the concentration in the bubble is rather uniform while in the liquid film large gradients of the concentration exist. These concentration gradients are sustained by the relative low mass transfer rate at the gas–liquid interface and by the large species consumption by the fast heterogeneous chemical reaction at the channel walls. Therefore, for this case the liquid film is never saturated and this region is very efficient for mass transfer, much more than the bubble top and bottom. As a consequence longer liquid films, i.e. longer unit cells, are more efficient for mass transfer for this case than short unit cells.

3.3. Influence of the liquid slug length

In order to investigate the influence of the liquid slug length on mass transfer, case D and E as listed in Table 3 are considered. The physical properties of the fluids are the same as in the previous section. Only the Henry number $H = 0.03$ is considered. The source term Π is adjusted so that a similar bubble velocity is obtained. As can be seen in Table 3, the bubbles have almost the same length, meaning that the contribution of the liquid film to mass transfer is similar. However, increasing the length of the liquid slug while keeping the bubble length about constant corresponds to a decrease of the gas hold-up ε, see Table 3. Also the bubble volume $V_B = \varepsilon L_{uc} d_h^2$ is different for case D and E. Since the initial concentration in the bubble is the same for both cases, namely $c_G^0 = 1$ mol/m^3, the initial amount of species within the unit cell $N_0 = V_B c_G^0$ is therefore about 10% higher in case D than in case E. In Fig. 10 we compare the time evolution of the normalized concentration in the gas and in the liquid for both cases. Because of the different values of ε, the non-dimensional equilibrium concentration in the gas and the liquid, evaluated with Eq. (23), is smaller for case E than for case D, see the horizontal lines in Fig. 10. Though at equilibrium in case E more species is transferred from the gas into the liquid phase simply because more liquid is available as solvent than in case D, the concentration in the liquid at equilibrium is higher for case D than for case E, see the inset graphics in Fig. 10. Thus, short liquid slugs are favourable for applications where the goal is to obtain a high concentration in the liquid phase within a short time interval, whereas long liquid slugs are favourable for applications where the focus is to transfer a large amount of species from the gas into the liquid phase.

The evaluation of the volumetric mass transfer coefficient for case D and E with Eq. (26) reveals that shorter liquid slugs are more

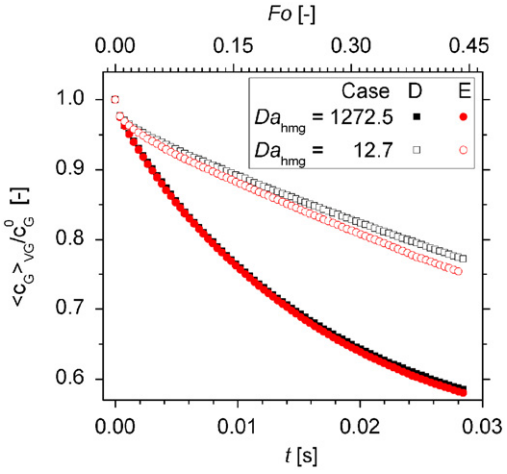

Fig. 11. Normalized mean gas concentration for mass transfer with homogeneous chemical reaction in the liquid phase for short (case D) and long (case E) liquid slug and two different values of the Damköhler number.

efficient for mass transfer than long liquid slugs. This result is in qualitative agreement with the experimental results of Berčič and Pintar (1997) for gas-to-liquid mass transfer in Taylor flow in circular capillaries. In that paper the importance of the liquid slug length is discussed and the volumetric mass transfer coefficient $k_L a$ is found to be proportional to $[(1-\varepsilon)L_{uc}]^{-0.57}$. Similar, Kreutzer et al. (2001) found from axisymmetric CFD computations that the mass transfer from the liquid slug to the wall is enhanced for short liquid slugs.

For mass transfer with species consumption by a homogeneous chemical reaction in the liquid phase two different values of the reaction constant are considered, namely $k_{hmg} = 198\,s^{-1}$ and $k_{hmg} = 19\,800\,s^{-1}$. These result in a Damköhler number $Da_{hmg} = 12.7$ for the slower reaction and $Da_{hmg} = 1272.5$ for the faster reaction. Fig. 11 shows that for the smaller value of Da_{hmg} slightly more species per time is transferred in the liquid phase for the long liquid slug (case E) than for the short liquid slug (case D). This result for the slow reaction may be explained by the equilibrium concentration for mass transfer without reaction, which is lower in case E than in case D, see Fig. 10. For the larger Damköhler number, the species consumption per unit time by the chemical reaction is much

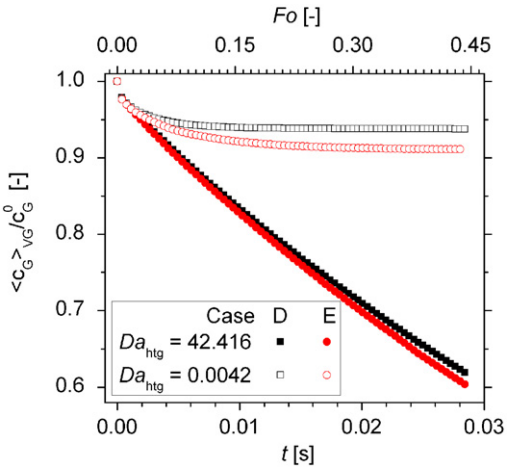

Fig. 12. Normalized mean gas concentration for short (case D) and long (case E) liquid slug for mass transfer with heterogeneous chemical reaction in the liquid phase and two different values of the Damköhler number.

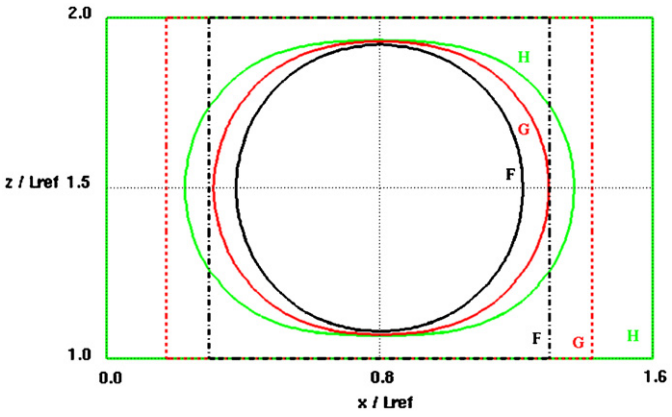

Fig. 13. Bubble shape in x–z cross section with largest bubble dimensions for case F, G and H. The boxes indicate the channel cross section for case F (dashed-dotted), G (dashed) and H (solid). Note that the size of the computational domain is non-dimensional and L_{ref} is different for each case.

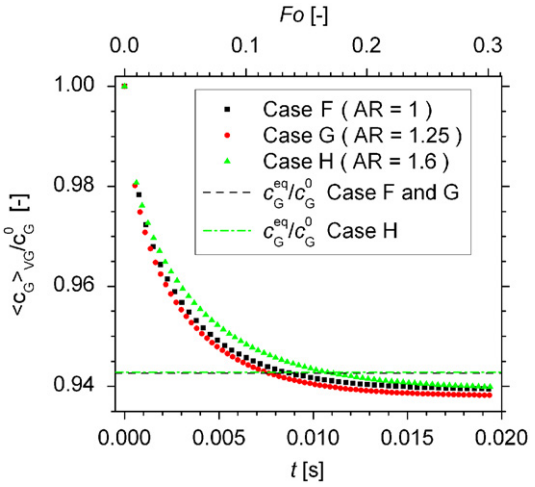

Fig. 14. Normalized mean gas concentration for mass transfer in rectangular channels with hydraulic diameter $d_h = 2$ mm and different values of the aspect ratio AR.

larger and the curves for case D and E in Fig. 11 are very similar. This suggests that a critical value of the Damköhler number may exist above which the influence of the liquid slug length becomes negligible for a homogeneous chemical reaction.

For the heterogeneous chemical reaction, the constant of the slower reaction was set to $k_{htg} = 1.32\times10^{-4}$ m/s and that of the faster one to $k_{htg} = 1.32$ m/s. The Damköhler number for the slower reaction is $Da_{htg} = 0.0042$, while for the fast reaction it is $Da_{htg} = 42.416$. The normalized mean gas concentration is displayed in Fig. 12. For the fast reaction the decrease of $\langle c_G(t)\rangle_{VG}/c_G^0$ over time is almost linear and the difference between the short and long liquid slug is very small, as it was also observed for the homogeneous reaction. Irandoust et al. (1989) performed experiments on mass transfer with heterogeneous reaction in a monolith catalyst reactor and found no influence of the liquid slug length. Our simulations results for the fast heterogeneous reaction are in qualitative agreement with their observation. For the slow reaction Fig. 12 shows that the initial decrease of $\langle c_G(t)\rangle_{VG}/c_G^0$ is of the same order as for the fast reaction. This is plausible, since this initial stage corresponds to the accumulation of species in the liquid bulk and its diffusion to the channel walls where the reaction takes place. For larger values of t, the decrease of $\langle c_G(t)\rangle_{VG}/c_G^0$ is very small for the slow reaction and the values are only slightly smaller than the corresponding equilibrium values in case of mass transfer without chemical reaction, see Fig. 10.

3.4. Influence of the channel aspect ratio

To investigate the influence of the channel cross section on mass transfer, three unit cell configurations having an aspect ratio ranging from 1 to 1.6 have been considered, see case F, G and H in Table 3. In order to facilitate a reasonable comparison between these cases, all three channels have the same hydraulic diameter $d_h = 2$ mm, the same gas content $\varepsilon \approx 33\%$, the same initial gas concentration $c_G^0 = 1$ mol/m^3 and the same initial amount of species in the gas phase. The pressure drop was adjusted to obtain in all cases the same value for the Peclet number $Pe_B \equiv Re_B Sc_L = d_h U_B/D_L$. Only the Henry number $H = 0.03$ is considered. For the constants of the homogeneous and heterogeneous chemical reaction, the same values as in Section 3.2 are used, namely $k_{hmg} = 19\,800\,s^{-1}$ and $k_{htg} = 1.32$ m/s. Gartsman et al. (1979) considered a chemical reaction to be fast if the ratio Da/Pe_B is larger than 10. Here, we have for the homogeneous reaction $Da_{hmg}/Pe_B = k_{hmg}d_h/U_B = 414.2$ and for the heterogeneous reaction $Da_{htg}/Pe_B = k_{htg}/U_B = 13.8$ so that both reactions can be considered as fast.

In Fig. 13 we compare for case F, G and H the cross-sectional bubble shape at that axial position, where the bubble dimensions are largest for each case. The bubble in the square channel has a circular cross-section, while in the rectangular channels the bubble is squeezed between the walls along the short side of the channel. Therefore, the fractional cross-sectional area of the channel occupied by the liquid film is increasing from case F to H, while the thickness of the liquid film relative to the smaller channel dimension is decreasing and that relative to the larger one is increasing. While the length of the bubble is about the same, the length of the liquid slug decreases from case F to H, see Table 3. However, the volumetric interfacial area concentration within the unit cell, $a = A_i/V_{uc}$, is about the same for all three channel aspect ratios.

The numerical results for the case of mass transfer without chemical reaction are displayed in Fig. 14 in terms of the normalized mean gas concentration. The horizontal lines denote the theoretical values of the normalized mean gas concentration at equilibrium according to Eq. (23). These values are almost the same for case F, G and H and thus the channel aspect ratio is without influence on the equilibrium concentrations. The results for $\langle c_G(t)\rangle_{VG}/c_G^0$ displayed in Fig. 14 are

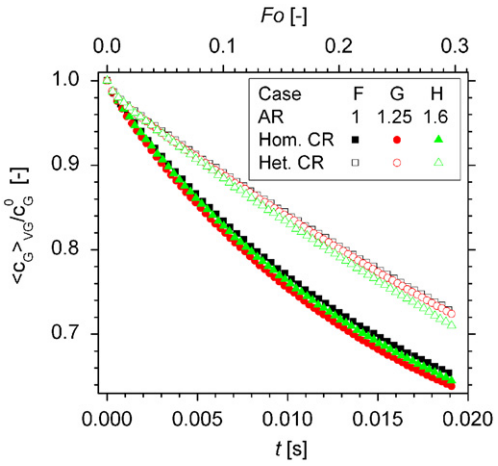

Fig. 15. Normalized mean gas concentration for mass transfer with homogeneous and heterogeneous chemical reaction in the liquid phase for rectangular channels with $d_h = 2$ mm and different values of the aspect ratio AR.

only slightly different for case F and G but nevertheless indicate, that the overall mass transfer in the 1.25 aspect ratio channel might be slightly more efficient than in the square channel. However, for case H with aspect ratio 1.6 the mass transfer is clearly less efficient as compared to case F and G, though the interfacial area concentration is about the same for all three cases. The reason may be that, for a given hydraulic diameter, the relative distance from the corners of the channel to the interface increases with increasing aspect ratio. Therefore, mass transfer to the corner regions may take more time.

The results for the normalized mean gas concentration for the case where the mass transfer is accompanied by a first-order chemical reaction are displayed in Fig. 15. It may appear surprising that for the second data point in Fig. 15 the value of $\langle c_G(t)\rangle_{VG}/c_G^0$ is the same for the homogeneous and heterogeneous chemical reaction. In general one would expect that the value of $\langle c_G(t)\rangle_{VG}/c_G^0$ is lower for the homogeneous reaction than for the heterogeneous reaction, since for the former case the species reacts in the liquid bulk while for the second case the species must diffuse to the wall before it can react. However, as mentioned above, for all cases with homogeneous reaction it is assumed that the reaction occurs only when the value $c_L/c_{ref} = 0.015$ is exceeded by the local concentration. For the homogeneous reaction, the mass transfer is most efficient for case G (aspect ratio 1.25) and least efficient for the square channel (case F) while case H with aspect ratio 1.6 is in between. At the moment, we do not have an explanation for this but note that for mass transfer with homogeneous reaction there is no clear trend for the dependence on the aspect ratio. In case of mass transfer with species consumption at the channel walls by a first-order heterogeneous chemical reaction, the results presented in Fig. 15 show that more mass is transferred in the liquid phase for the channels with large aspect ratio. The flow within these channels takes advantage of the decreasing thickness of the liquid film along the short side of the channel and the increasing bubble lateral surface in close proximity to the wall. This result signifies that, for the same hydraulic diameter, rectangular channels may be more suitable for monoliths with catalytic walls than square channels. Nevertheless, this conjecture should be verified by experimental investigations.

4. Conclusions

In this paper we presented a finite volume-based VOF method for numerical simulation of conjugate mass transfer of a dilute species with resistance in both phases across a fluid interface. The method takes into account the concentration jump at the interface according to Henrys law by transforming the discontinuous physical concentration field in a continuous numerical one. A common drawback of such a transformation is that the mass flux formulated in terms of the transformed concentration is discontinuous across the interface, while the physical mass flux is continuous. In the new method this drawback is circumvented by an appropriate modification of the cell face diffusivities in such a way that the continuity of the physical diffusive mass flux across the interface is fulfilled. This makes the method suitable for arbitrary values of the equilibrium distribution coefficient (respectively, Henry number), though for values $H > 1$ very fine grids are required. A special feature of this method is that it cannot only compute mass transfer from high to low concentration but also from low to high concentration, depending on the equilibrium concentrations at the interface. The numerical method has been validated by comparison to one and two-dimensional diffusive mass transfer problems with known solutions.

The method has been implemented in an in-house VOF computer code with piecewise linear interface reconstruction and has been used to compute the mass transfer of a dilute species from the gas into the liquid phase in co-current vertical bubble train flow within square and rectangular mini-channels with optional first-order homogeneous or heterogeneous chemical reaction. Only one unit cell of the bubble train flow is considered with periodic boundary conditions in axial direction. The diffusivity of the species in the liquid phase is arbitrarily increased so that the Schmidt number for the liquid phase is 0.8. In a series of simulations the qualitative influence of the unit cell length, the liquid slug length and the channel aspect ratio on the efficiency of mass transfer is studied. It turned out that for interpretation of the results the degree of saturation of the liquid film is of great importance, which can be quantified in terms of the exposure time Fourier number Fo_{exp}. When there is no chemical reaction and Fo_{exp} is large as it is in the present simulations, the liquid film is quickly saturated and the lateral sides of the bubble and the liquid film become inactive for mass transfer. In this case most of the mass is transferred through the cap and bottom of the bubble so that short unit cells are more efficient for mass transfer. The variation of the liquid slug length revealed that long liquid slugs are more efficient for applications where the focus is on the transfer of a large amount of species from the gas into the liquid phase, while short liquid slugs are favourable when a high concentration in the continuous phase is of interest.

In case of species consumption by a homogeneous chemical reaction, the qualitative influence of the unit cell length is the same as for mass transfer only, namely short unit cells are more efficient. If the chemical reaction is fast, then the liquid slug length is without influence on the efficiency of the mass transfer, both for the homogeneous and the heterogeneous reaction. In case of a fast heterogeneous reaction and when the main resistance to mass transfer is in the gas phase it appears, however, that long unit cells are more efficient since then there is a sustained large concentration gradient in the liquid film between the bubble and the channel wall. This is also the reason why in the study of the influence of the channel aspect ratio it was found that—for the same hydraulic channel diameter—a large aspect ratio appears to be favourable for fast heterogeneous chemical reactions, e.g. in monolith reactors.

In the present paper the mass transfer of an artificial species at a Schmidt number of order one has been considered. In practical applications the Schmidt number is usually much larger and the liquid film will in general not be saturated. The present numerical method is not restricted with respect to the value of the Schmidt number, however, an adequate resolution of the thin concentration boundary layer is essential and much finer grids are required than have been used here. Our next goal is, therefore, to use the code to investigate mass transfer in bubble train flow for conditions that exhibit no liquid film saturation and to consider higher values of the

Schmidt number, as well as to perform a quantitative validation of the code for mass transfer in bubble train flow.

Notation

a	volumetric interfacial area concentration in the unit cell, m^2/m^3
a_i	local non-dimensional volumetric interfacial area concentration normalized by L_{ref}, dimensionless
A_i	bubble interfacial area, m^2
c	concentration, mol/m^3
Ca	capillary number, dimensionless
d	diameter, m
D	diffusion coefficient, m^2/s
Da	Damköhler number, dimensionless
$Eö$	Eötvös number, dimensionless
Eu	Euler number, dimensionless
f	liquid volumetric fraction, dimensionless
F	factor for computation of cell face mixture diffusivity, dimensionless
Fo	Fourier number, dimensionless
Fo_{exp}	Fourier number based on exposure time, dimensionless
Fr	Froude number, dimensionless
g	gravitational acceleration, m/s^2
G	factor for computation of cell face mixture diffusivity, dimensionless
H	Henry number, $H \equiv c_L^{eq}/c_G^{eq}$, dimensionless
i, j, k	mesh cell indices, dimensionless
$\mathbf{j}$	molar flux, $mol/m^2\,s$
J	total superficial velocity, m/s
k_{hmg}	constant of homogeneous reaction, s^{-1}
k_{htg}	constant of heterogeneous reaction, m/s
k_L	mass transfer coefficient, m/s
L	length, m
Mo	Morton number, dimensionless
$\hat{\mathbf{n}}_i$	unit normal vector to the interface pointing into the liquid, dimensionless
N	species mass, mol
p	pressure, Pa
r	sink term for homogeneous chemical reaction, $mol/m^3\,s$
Re	Reynolds number, dimensionless
Sc	Schmidt number (continuous phase), dimensionless
t	time, s
Δt	time step width, s
U	velocity, m/s
$\mathbf{v}$	velocity field, m/s
V	volume, m^3
We	Weber number, dimensionless
x, y, z	Cartesian coordinates, m

Greek letters

δ	Dirac delta function, dimensionless
δ_{LF}	lateral thickness of the liquid film, m
ε	gas volume fraction, dimensionless
θ	non-dimensional time, dimensionless
κ	interface curvature made non-dimensional by L_{ref}, dimensionless
λ	factor for computation of cell face mixture diffusivity, dimensionless
μ	dynamic viscosity, Pa s
Π	source term in momentum equation, dimensionless
ρ	density, kg/m^3
σ	surface tension, N/m

Subscripts and superscripts

0	initial state
B	bubble
eq	equilibrium
exp	exposure
G	gas phase ($k = 2$)
h	hydraulic
hmg	homogeneous
htg	heterogeneous
i	interface
k	phase index ($k = 1, 2$)
L	liquid phase ($k = 1$)
LF	liquid film
LS	liquid slug
m	mixture quantity
ref	reference
uc	unit cell

Acknowledgements

The authors thank Prof. D. Bothe for providing the Mathematica file with the theoretical solution for the two-dimensional mass transfer test case used for code verification. They also thank Mr. S. Kececi for performing the simulation for the grid refinement study and the reviewers for useful comments.

Appendix A. Derivation of volume averaged species transport equation

We denote by subscript $k = 1,2$ two immiscible fluid phases that reside in domains $\Omega_k(t)$ and are separated by an interface $S_i(t)$. The mass conservation equation for a chemical species valid within each phase can then be written in the non-dimensional form

$$\frac{\partial c_k/c_{ref}}{\partial \theta} + \nabla \cdot \left(\frac{c_k}{c_{ref}} \frac{\mathbf{v}_k}{U_{ref}} \right) = -\frac{1}{Re_{ref} Sc_{ref}} \nabla \cdot \mathbf{j}_k - \frac{t_{ref}}{c_{ref}} r_k \quad \text{for } \mathbf{x} \in \Omega_k \tag{A.1}$$

Here, the reference scales L_{ref}, U_{ref} , $t_{ref} \equiv L_{ref}/U_{ref}$ and c_{ref} are used for normalization and the non-dimensional diffusive mass flux is given by

$$\mathbf{j}_k \equiv -(D_k/D_{ref})\nabla(c_k/c_{ref}) \quad \text{for } \mathbf{x} \in \Omega_k \tag{A.2}$$

At the interface the concentrations on both sides are related by Henry's law

$$c_{1i} = Hc_{2i} \quad \text{for } \mathbf{x} \in S_i \tag{A.3}$$

and the mass fluxes are equal

$$\mathbf{j}_{1i} \cdot \hat{\mathbf{n}}_1 + \mathbf{j}_{2i} \cdot \hat{\mathbf{n}}_2 = (\mathbf{j}_{1i} - \mathbf{j}_{2i}) \cdot \hat{\mathbf{n}}_i = 0 \quad \text{for } \mathbf{x} \in S_i \tag{A.4}$$

Here, $\hat{\mathbf{n}}_i \equiv \hat{\mathbf{n}}_1 = -\hat{\mathbf{n}}_2$ is the unit normal vector to the interface pointing into the continuous phase ($k = 1$). We further define two phase indicator functions

$$X_k(\mathbf{x}, t) = \begin{cases} 1, & \mathbf{x} \in \Omega_k(t) \\ 0 & \text{otherwise} \end{cases} \tag{A.5}$$

and the two volume averaging operators

$$\overline{\varphi_k}^V \equiv \frac{1}{V}\int\int\int_V \varphi_k X_k \,\mathrm{d}V, \quad \overline{\varphi_k}^k \equiv \frac{1}{\alpha_k V}\int\int\int_V \varphi_k X_k \,\mathrm{d}V \tag{A.6}$$

where $\alpha_k \equiv \overline{X_k}^V$ and $\overline{\varphi_k}^k$ represents the intrinsic phase average of φ.

In order to obtain an equation that is valid throughout the entire domain $\Omega = \Omega_1 \cup \Omega_2$, we multiply Eq. (A.1) by X_k and perform the averaging over volume V. Assuming a first-order homogeneous chemical reaction with $r_k = k_k^{\mathrm{hmg}} c_k$ and a constant reaction rate k_k^{hmg} gives

$$\overline{X_k \frac{\partial c_k/c_{\mathrm{ref}}}{\partial\theta}}^V + \overline{X_k \nabla\cdot\left(\frac{c_k}{c_{\mathrm{ref}}}\frac{\mathbf{v}_k}{U_{\mathrm{ref}}}\right)}^V = -\frac{1}{Re_{\mathrm{ref}}Sc_{\mathrm{ref}}}\overline{X_k\nabla\cdot\mathbf{j}_k}^V - \frac{L_{\mathrm{ref}}k_k^{\mathrm{hmg}}}{U_{\mathrm{ref}}}\overline{X_k\frac{c_k}{c_{\mathrm{ref}}}}^V \tag{A.7}$$

For the first term on the l.h.s. of Eq. (A.7) we obtain from the Leibniz rule for volume averaging (Drew and Passman, 1999) the result

$$\begin{aligned}\overline{X_k \frac{\partial c_k/c_{\mathrm{ref}}}{\partial\theta}}^V &= \frac{\partial}{\partial\theta}\overline{X_k\frac{c_k}{c_{\mathrm{ref}}}}^V + \overline{\frac{c_k}{c_{\mathrm{ref}}}\frac{\mathbf{v}_{\mathrm{i}}}{U_{\mathrm{ref}}}\cdot\nabla X_k}^V \\ &= \frac{\partial}{\partial\theta}\frac{\alpha_k\overline{c_k}^k}{c_{\mathrm{ref}}} + \overline{\frac{c_k}{c_{\mathrm{ref}}}\frac{\mathbf{v}_{\mathrm{i}}}{U_{\mathrm{ref}}}\cdot\nabla X_k}^V\end{aligned} \tag{A.8}$$

where $\mathbf{v}_{\mathrm{i}}$ represents the velocity of the interface. Using the Gauss rule for volume averaging (Drew and Passman, 1999), the second term on the l.h.s. of Eq. (A.7), as well as the diffusive flux term can be expressed as

$$\begin{aligned}\overline{X_k\nabla\cdot\left(\frac{c_k}{c_{\mathrm{ref}}}\frac{\mathbf{v}_k}{U_{\mathrm{ref}}}\right)}^V &= \nabla\cdot\overline{X_k\frac{c_k}{c_{\mathrm{ref}}}\frac{\mathbf{v}_k}{U_{\mathrm{ref}}}}^V - \overline{\frac{c_k}{c_{\mathrm{ref}}}\frac{\mathbf{v}_{\mathrm{ki}}}{U_{\mathrm{ref}}}\cdot\nabla X_k}^V \\ &= \nabla\cdot\alpha_k\overline{\frac{c_k}{c_{\mathrm{ref}}}\frac{\mathbf{v}_k}{U_{\mathrm{ref}}}}^k - \overline{\frac{c_k}{c_{\mathrm{ref}}}\frac{\mathbf{v}_{\mathrm{ki}}}{U_{\mathrm{ref}}}\cdot\nabla X_k}^V\end{aligned} \tag{A.9}$$

$$\overline{X_k\nabla\cdot\mathbf{j}_k}^V = \nabla\cdot\overline{X_k\mathbf{j}_k}^V - \overline{\mathbf{j}_{\mathrm{ki}}\cdot\nabla X_k}^V = \nabla\cdot\alpha_k\overline{\mathbf{j}_k}^k - \overline{\mathbf{j}_{\mathrm{ki}}\cdot\nabla X_k}^V \tag{A.10}$$

Here, $\mathbf{v}_{\mathrm{ki}}$ and $\mathbf{j}_{\mathrm{ki}}$ represent the velocity and the diffusive flux on the k-side of the interface. Introducing the terms (A.8)–(A.10) in Eq. (A.7) gives

$$\begin{aligned}&\frac{\partial}{\partial\theta}\frac{\alpha_k\overline{c_k}^k}{c_{\mathrm{ref}}} + \nabla\cdot\left(\alpha_k\overline{\frac{c_k}{c_{\mathrm{ref}}}\frac{\mathbf{v}_k}{U_{\mathrm{ref}}}}^k\right) \\ &= -\frac{1}{Re_{\mathrm{ref}}Sc_{\mathrm{ref}}}\left[\nabla\cdot\alpha_k\overline{\mathbf{j}_k}^k - \overline{\mathbf{j}_{\mathrm{ki}}\cdot\nabla X_k}^V\right] \\ &\quad - \alpha_k\frac{L_{\mathrm{ref}}k_k^{\mathrm{hmg}}}{U_{\mathrm{ref}}}\frac{\overline{c_k}^k}{c_{\mathrm{ref}}} + \overline{\frac{c_k}{c_{\mathrm{ref}}}\frac{\mathbf{v}_{k_{\mathrm{i}}}-\mathbf{v}_{\mathrm{i}}}{U_{\mathrm{ref}}}\cdot\nabla X_k}^V\end{aligned} \tag{A.11}$$

The last term in the above equation is associated with the mass transfer across the interface due to phase change. In this paper, we do not consider phase change. Therefore, the velocity at the interface is continuous ($\mathbf{v}_{1\mathrm{i}} = \mathbf{v}_{2\mathrm{i}} = \mathbf{v}_{\mathrm{i}}$) and the last term in Eq. (A.11) vanishes. The convective term on the l.h.s. of Eq. (A.11) is nonlinear and gives rise to turbulent mass fluxes. Introducing the conventional splits of large-eddy-simulation in a volumetric mean value and a deviation from the mean value, i.e. $c_k' \equiv c_k - \overline{c_k}^k$ and $\mathbf{v}_k' \equiv \mathbf{v}_k - \overline{\mathbf{v}_k}^k$, gives rise to the sub-grid scale terms

$$\begin{aligned}\overline{c_k\mathbf{v}_k}^k \equiv \overline{c_k}^k\overline{\mathbf{v}_k}^k + \mathbf{q}_k^{\mathrm{sgs}} &= \overline{c_k}^k\overline{\mathbf{v}_k}^k + \underbrace{\left(\overline{\overline{c_k}^k\overline{\mathbf{v}_k}^k}^k - \overline{c_k}^k\overline{\mathbf{v}_k}^k\right)}_{\mathbf{q}_k^{\mathrm{L}}} \\ &\quad + \underbrace{\left(\overline{c_k'\overline{\mathbf{v}_k}^k}^k - \overline{\overline{c_k}^k\mathbf{v}_k'}^k\right)}_{\mathbf{q}_k^{\mathrm{C}}} + \underbrace{\overline{c_k'\mathbf{v}_k'}^k}_{\mathbf{q}_k^{\mathrm{R}}}\end{aligned} \tag{A.12}$$

In analogy with the analysis of the volume averaged momentum equation, the vectors $\mathbf{q}_k^{\mathrm{L}}$, $\mathbf{q}_k^{\mathrm{C}}$ and $\mathbf{q}_k^{\mathrm{R}}$ are designated as sub-grid scale Leonard-like term, sub-grid scale cross-term and sub-grid scale Reynolds-like stress term. In general, appropriate sub-grid scale closure assumptions have to be employed to model $\mathbf{q}_k^{\mathrm{sgs}}$. Whitaker (1973) designates the last term in Eq. (A.12) as the dispersion vector and proposes a representation in form of a diffusion mechanism. It is reported that the time-dependant dispersion coefficient is strongly dependant on the concentration gradient. Nevertheless, unsatisfactory results were obtained for dispersion at short times or high concentration gradient. Within this paper we assume that the grid is sufficiently fine to resolve all scales of the velocity and concentration field, so that $\mathbf{q}_k^{\mathrm{sgs}}$ can be neglected.

We further define $H_1 = 1$ and $H_2 = H$, where H is the Henry number. Multiplying Eq. (A.11) by H_k and summing up the respective equations for $k = 1$ and for $k = 2$ gives

$$\begin{aligned}&\sum_{k=1}^{2}\left[\frac{\partial}{\partial\theta}H_k\alpha_k\frac{\overline{c_k}^k}{c_{\mathrm{ref}}} + \nabla\cdot H_k\alpha_k\frac{\overline{c_k}^k}{c_{\mathrm{ref}}}\frac{\overline{\mathbf{v}_k}^k}{U_{\mathrm{ref}}}\right] \\ &= -\frac{1}{Re_{\mathrm{ref}}Sc_{\mathrm{ref}}}\sum_{k=1}^{2}[\nabla\cdot H_k\alpha_k\overline{\mathbf{j}_k}^k - H_k\overline{\mathbf{j}_{\mathrm{ki}}\cdot\nabla X_k}^V] \\ &\quad - \sum_{k=1}^{2}H_k\alpha_k\frac{L_{\mathrm{ref}}k_k^{\mathrm{hmg}}}{U_{\mathrm{ref}}}\frac{\overline{c_k}^k}{c_{\mathrm{ref}}}\end{aligned} \tag{A.13}$$

In the following we assume that the homogenous chemical reaction occurs only in the continuous phase so that $k_2^{\mathrm{hmg}} = 0$ and $k_1^{\mathrm{hmg}} = k_{\mathrm{hmg}}$. Then, the last term in Eq. (A.13) becomes

$$\sum_{k=1}^{2}H_k\alpha_k\frac{L_{\mathrm{ref}}k_k^{\mathrm{hmg}}}{U_{\mathrm{ref}}}\frac{\overline{c_k}^k}{c_{\mathrm{ref}}} = \alpha_1\frac{L_{\mathrm{ref}}k_{\mathrm{hmg}}}{U_{\mathrm{ref}}}\frac{\overline{c_1}^1}{c_{\mathrm{ref}}} = \frac{Da_{\mathrm{ref}}^{\mathrm{hmg}}}{Re_{\mathrm{ref}}Sc_{\mathrm{ref}}}\alpha_1\frac{\overline{c_1}^1}{c_{\mathrm{ref}}} \tag{A.14}$$

where $Da_{\mathrm{ref}}^{\mathrm{hmg}}$ is the reference Damköhler number defined by Eq. (14).

With index $k = 1$ representing the (continuous) liquid phase ($c_{\mathrm{L}} = \overline{c_1}^1$), index $k = 2$ the (disperse) gas phase ($c_{\mathrm{G}} = \overline{c_2}^2$), $f \equiv \alpha_1$ and with the definitions (5), (7) and (12) we can rewrite the sum of the convective term as

$$\sum_{k=1}^{2}H_k\alpha_k\frac{\overline{c_k}^k}{c_{\mathrm{ref}}}\frac{\overline{\mathbf{v}_k}^k}{U_{\mathrm{ref}}} = c_{\mathrm{m}}\mathbf{v}_{\mathrm{m}} + \frac{\alpha_1\alpha_2}{\rho_{\mathrm{m}}}\left(H\frac{c_{\mathrm{G}}}{c_{\mathrm{ref}}} - \frac{\rho_2}{\rho_1}\frac{c_{\mathrm{L}}}{c_{\mathrm{ref}}}\right)\mathbf{v}_{\mathrm{r}}, \tag{A.15}$$

where $\mathbf{v}_{\mathrm{r}} \equiv (\overline{\mathbf{v}_2}^2 - \overline{\mathbf{v}_1}^1)/U_{\mathrm{ref}}$ is the non-dimensional mean relative velocity between the phases in the averaging volume, i.e. the mesh cell. Here we assume that the hydrodynamic boundary layers on both sides of the interface are well resolved by the grid so that

$\mathbf{v}_r = 0$. Then, Eq. (A.13) becomes

$$\frac{\partial c_m}{\partial \theta} + \nabla \cdot c_m \mathbf{v}_m = -\frac{1}{Re_{ref} Sc_{ref}} \left[\nabla \cdot \sum_{k=1}^{2} H_k \alpha_k \overline{\mathbf{j}_k}^k - \sum_{k=1}^{2} H_k \overline{\mathbf{j}_{ki} \cdot \nabla X_k}^V + Da_{ref}^{hmg} f \frac{c_L}{c_{ref}} \right] \tag{A.16}$$

We next consider the two diffusive terms in Eq. (A.16). The first term

$$\mathbf{j}_m \equiv \sum_{k=1}^{2} H_k \alpha_k \overline{\mathbf{j}_k}^k = -\sum_{k=1}^{2} H_k \alpha_k \frac{D_k}{D_{ref}} \nabla \frac{\overline{c_k}^k}{c_{ref}} = -f \frac{D_L}{D_{ref}} \nabla \frac{c_L}{c_{ref}} - (1-f) \frac{D_G}{D_{ref}} \nabla \frac{H c_G}{c_{ref}} \tag{A.17}$$

shall be expressed in terms of c_m. In liquid filled cells ($f = 1$) we have $c_L/c_{ref} = c_m$, while in gas filled cells ($f = 0$) we have $Hc_G/c_{ref} = c_m$. For interface cells ($0 < f < 1$) we assume that the concentrations are in thermodynamic equilibrium, so that $c_L/c_{ref} = Hc_G/c_{ref} = c_m$. Therefore we can write

$$\mathbf{j}_m = -\frac{f D_L + (1-f) D_G}{D_{ref}} \nabla c_m = -\frac{D_m}{D_{ref}} \nabla c_m \tag{A.18}$$

We now consider the second term in the brackets of Eq. (A.16), which is the volume average of the jump condition of $\mathbf{j}_m$ across the interface, which reads

$$\begin{aligned} &- \frac{D_1}{D_{ref}} \nabla \frac{c_1}{c_{ref}}\bigg|_{1i} \cdot \hat{\mathbf{n}}_1 - \frac{D_2}{D_{ref}} \nabla \frac{H c_2}{c_{ref}}\bigg|_{2i} \cdot \hat{\mathbf{n}}_2 \\ &= -\sum_{k=1}^{2} \frac{D_k}{D_{ref}} \nabla \frac{H_k c_k}{c_{ref}}\bigg|_{ki} \cdot \hat{\mathbf{n}}_k \\ &= \sum_{k=1}^{2} H_k \mathbf{j}_{ki} \cdot \hat{\mathbf{n}}_k = \sum_{k=1}^{2} H_k \mathbf{j}_{ki} \cdot \nabla X_k \end{aligned} \tag{A.19}$$

Here we made use of relation $\nabla X_k = \hat{\mathbf{n}}_k \delta(\mathbf{x} - \mathbf{x}_i, t)$, where δ is the Dirac delta function and $\mathbf{x}_i$ is the position vector to any point on the interface. Multiplying Eq. (A.4) by $\delta(\mathbf{x} - \mathbf{x}_i, t)$ and subsequent volume averaging gives

$$\overline{\mathbf{j}_{1i} \cdot \nabla X_1}^V + \overline{\mathbf{j}_{2i} \cdot \nabla X_2}^V = \sum_{k=1}^{2} \overline{\mathbf{j}_{ki} \cdot \nabla X_k}^V = 0 \tag{A.20}$$

Using the latter results, we obtain for the second term in brackets on the r.h.s. of Eq. (A.16)

$$\begin{aligned} &\sum_{k=1}^{2} H_k \overline{\mathbf{j}_{ki} \cdot \nabla X_k}^V \\ &= \overline{\mathbf{j}_{1i} \cdot \nabla X_1}^V + H \overline{\mathbf{j}_{2i} \cdot \nabla X_2}^V = (H-1) \overline{\mathbf{j}_{2i} \cdot \nabla X_2}^V \\ &= (1-H) \overline{\mathbf{j}_{1i} \cdot \nabla X_1}^V = (1-H) \frac{1}{V} \int \int_{Si \cap V} \mathbf{j}_{1i} \cdot \hat{\mathbf{n}}_1 \, dS \\ &= -(1-H) \frac{a_i}{S_i} \int \int_{Si \cap V} \frac{D_L}{D_{ref}} \frac{\partial c_L / c_{ref}}{\partial n}\bigg|_{Li} dS = (1-H) a_i \overline{j_{GL}}^{S_i} \end{aligned} \tag{A.21}$$

Here, $a_i \equiv S_i/V$ is the local volumetric interfacial area concentration and $\overline{j_{GL}}^{S_i}$ is the mean non-dimensional mass flux on the liquid side of the interface (counted positive when the mass flux is from the gas side to the liquid side). Whitaker (1973, 1999) denotes the term $\overline{\mathbf{j}_{ki} \cdot \nabla X_k}^V$ as diffusive interface transport term. Inserting (A.21) in Eq. (A.16) yields the non-dimensional volume averaged species conservation equation in the final form

$$\frac{\partial c_m}{\partial \theta} + \nabla \cdot c_m \mathbf{v}_m = -\frac{1}{Re_{ref} Sc_{ref}} \left[\nabla \cdot \mathbf{j}_m + \underbrace{(H-1) a_i \overline{j_{GL}}^{S_i}}_{\equiv Q_i} + Da_{ref}^{hmg} f \frac{c_L}{c_{ref}} \right] \tag{A.22}$$

Similar to the surface tension term in the volume averaged momentum equation, the term Q_i is proportional to the local volumetric interfacial area concentration a_i. Thus, Q_i is non-zero only in mesh cells containing the interface.

Appendix B. Derivation of formula for cell face mixture diffusivity

We consider a grid that is optionally non-uniform in x-direction (index i, grid width Δx_i), but is uniform in y- and z-direction (index j and k, respectively). We further consider two neighbouring mesh cells with index (i,j,k) and ($i+1,j,k$) that share a common face (index $i+1/2$). Our goal is to express the non-dimensional diffusive mass flux across this common face in terms of the concentration c_m in the form

$$j_{i+1/2,j,k} = D_{m;i+1/2,j,k} \frac{c_{m;i+1,j,k} - c_{m;i,j,k}}{(\Delta x_i + \Delta x_{i+1})/2} \tag{B.1}$$

We determine $D_{m;i+1/2,j,k}$ from the restriction that the physical mass flux across the interface must be equal for both sides of the interface. We follow the procedure of Patankar (1980) and assume for the moment that $f_{i,j,k} = 1$ and $f_{i+1,j,k} = 0$ so that the interface is located exactly at the common face of both mesh cells. The physical diffusive mass fluxes at cell face $i+1/2$ can be expressed in terms of the concentration c_m as

$$j^L_{i+1/2,j,k} = D_{i,j,k} \frac{c_{m;i+1/2,j,k} - c_{m;i,j,k}}{\Delta x_i/2} \tag{B.2}$$

$$j^G_{i+1/2,j,k} = \frac{D_{i+1,j,k}}{H} \frac{c_{m;i+1,j,k} - c_{m;i+1/2,j,k}}{\Delta x_{i+1}/2} \tag{B.3}$$

where the non-dimensional diffusivities are, for the interface location mentioned above, given by $D_{i,j,k} = 1$ and $D_{i+1,j,k} = D_G/D_L$.

Since both fluxes are equal one can obtain from Eqs. (B.2) and (B.3) the following result for the fictitious concentration at the common cell face $i+1/2$

$$c_{m;i+1/2,j,k} = \frac{D_{i,j,k} \frac{c_{m;i,j,k}}{\Delta x_i} + \frac{D_{i+1,j,k}}{H} \frac{c_{m;i+1,j,k}}{\Delta x_{i+1}}}{\frac{D_{i,j,k}}{\Delta x_i} + \frac{1}{H} \frac{D_{i+1,j,k}}{\Delta x_{i+1}}} \tag{B.4}$$

Inserting this result in Eq. (B.2) or (B.3) we obtain for the diffusive flux at the interface the result

$$j_{i+1/2,j,k} = j^L_{i+1/2,j,k} = j^G_{i+1/2,j,k} = 2 \frac{c_{m;i+1,j,k} - c_{m;i,j,k}}{\Delta x_i / D_{m;i,j,k} + H \Delta x_{i+1} / D_{m;i+1,j,k}} \tag{B.5}$$

Comparing this equation with Eq. (B.1) yields the required result for $D_{m;i+1/2,j,k}$, namely

$$D_{m;i+1/2,j,k} = \frac{\Delta x_i + \Delta x_{i+1}}{\Delta x_i / D_{i,j,k} + H \Delta x_{i+1} / D_{i+1,j,k}} \tag{B.6}$$

Similarly, we obtain for the case where $f_{i,j,k} = 0$ and $f_{i+1,j,k} = 1$ the result

$$D_{m;i+1/2,j,k} = \frac{\Delta x_i + \Delta x_{i+1}}{H \Delta x_i / D_{i,j,k} + \Delta x_{i+1} / D_{i+1,j,k}} \tag{B.7}$$

To compute $D_{m;i+1/2,j,k}$ for general values of $f_{i,j,k}$ and $f_{i+1,j,k}$, i.e. arbitrary locations and orientations of the interface, we generalize Eqs. (B.6) and (B.7) as

$$D_{m;i+1/2,j,k} = \frac{\Delta x_i + \Delta x_{i+1}}{F_{i+1/2,j,k}\Delta x_i/D_{m;i,j,k} + G_{i+1/2,j,k}\Delta x_{i+1}/D_{m;i+1,j,k}} \tag{B.8}$$

where $D_{m;i,j,k}$ is the cell centred mixture diffusivity defined by Eq. (16). The conditions for setting $F_{i+1/2,j,k}$ and $G_{i+1/2,j,k}$ either to 1 or H are given in Table 1, where Eq. (B.8) is given for the special case when the grid is uniform.

Appendix C. Derivation of formulation for mass transfer coefficient

We consider a unit cell where the initial amount of species in the gas phase is $N_G(t=0)=N_G^0$, while the initial amount of species in the liquid phase is zero. The time-dependant amount of species in the gas phase is $N_G(t)$ and that in the liquid phase is $N_L(t)=N_G^0-N_G(t)$. The time-dependant normalized mean concentration in the gas is then given by $\langle c_G(t)\rangle_{VG}=N_G(t)/N_G^0$ and that in the liquid by

$$\frac{\langle c_L(t)\rangle_{V_L}}{c_G^0} = \frac{N_G^0 - N_G(t)}{(1-\varepsilon)V_{uc}}\frac{\varepsilon V_{uc}}{N_G^0} = \frac{\varepsilon}{1-\varepsilon}\left(1 - \frac{\langle c_G(t)\rangle_{VG}}{c_G^0}\right) \tag{C.1}$$

We define mass transfer coefficients for the gas and liquid side as

$$k_G(t) \equiv \frac{\dot N_G(t)/A_i}{c_{G,bulk} - c_{G,i}} = \frac{\dot n_G(t)}{\langle c_G(t)\rangle_{VG} - \langle c_G(t)\rangle_{A_i}} \tag{C.2}$$

$$k_L(t) \equiv \frac{\dot N_L(t)/A_i}{c_{L,i} - c_{L,bulk}} = \frac{\dot n_L(t)}{\langle c_L(t)\rangle_{A_i} - \langle c_L(t)\rangle_{VL}} \tag{C.3}$$

where $\langle c_G(t)\rangle_{Ai}$ and $\langle c_L(t)\rangle_{Ai}$ denote the surface-averaged concentrations of the gas and liquid side of the interface, respectively. With the assumption that the mean concentrations on both sides of the interface are in equilibrium, i.e. $\langle c_L(t)\rangle_{Ai} = H\langle c_G(t)\rangle_{Ai}$, and with $\dot n_G(t) = \dot n_L(t) = \dot n(t)$ we obtain from Eqs. (C.2) and (C.3) the result

$$\dot n(t) = \frac{H\langle c_G(t)\rangle_{VG} - \langle c_L(t)\rangle_{VL}}{\dfrac{H}{k_G(t)} + \dfrac{1}{k_L(t)}} \tag{C.4}$$

From this equation, depending on the choice for the driving concentration difference, two different overall mass transfer coefficients can be defined, namely

$$k_{ov}^L(t) \equiv \left(\frac{H}{k_G(t)} + \frac{1}{k_L(t)}\right)^{-1} = \frac{\dot n(t)}{H\langle c_G(t)\rangle_{VG} - \langle c_L(t)\rangle_{VL}} = \frac{\dfrac{\dot n(t)}{c_G^0}}{H\dfrac{\langle c_G(t)\rangle_{VG}}{c_G^0} - \dfrac{\langle c_L(t)\rangle_{VL}}{c_G^0}} \tag{C.5}$$

and

$$k_{ov}^G(t) \equiv \left(\frac{1}{k_G(t)} + \frac{1}{Hk_L(t)}\right)^{-1} = \frac{\dot n(t)}{\langle c_G(t)\rangle_{VG} - \dfrac{1}{H}\langle c_L(t)\rangle_{VL}} = \frac{\dfrac{\dot n(t)}{c_G^0}}{\dfrac{\langle c_G(t)\rangle_{VG}}{c_G^0} - \dfrac{1}{H}\dfrac{\langle c_L(t)\rangle_{VL}}{c_G^0}} \tag{C.6}$$

Both mass transfer coefficients are related by $k_{ov}^G(t) = Hk_{ov}^L(t)$. The nominator of Eq. (C.6) is given by

$$\frac{\dot n(t)}{c_G^0} = \frac{\dot N(t)}{A_i c_G^0} = \frac{1}{A_i c_G^0}\frac{dN_L(t)}{dt} = -\frac{1}{A_i c_G^0}\frac{dN_G(t)}{dt} = -\frac{\varepsilon V_{uc}}{A_i}\frac{d}{dt}\frac{\langle c_G(t)\rangle_{VG}}{c_G^0} = -\frac{\varepsilon}{a_i}\frac{d}{dt}\frac{\langle c_G(t)\rangle_{VG}}{c_G^0} \tag{C.7}$$

while for the denominator it follows from Eq. (C.1) the result

$$\frac{\langle c_G(t)\rangle_{VG}}{c_G^0} - \frac{1}{H}\frac{\langle c_L(t)\rangle_{VL}}{c_G^0} = \frac{\langle c_G(t)\rangle_{VG}}{c_G^0}\left(1 + \frac{\varepsilon}{H(1-\varepsilon)}\right) - \frac{\varepsilon}{H(1-\varepsilon)} \tag{C.8}$$

Substituting Eqs. (C.7) and (C.8) in Eq. (C.6) we obtain for the overall mass transfer coefficient the result given by Eq. (26). We note that for large times $\langle c_G(t)\rangle_{VG}/c_G^0$ approaches the constant equilibrium value given by Eq. (23). Then, both the nominator (C.7) and the denominator (C.8) tend to zero.

References

Apelblat, A., 1980. Mass transfer with a chemical reaction of the first order: analytical solutions. Chemical Engineering Journal 19, 19–37.

Berčič, G., Pintar, A., 1997. The role of gas bubbles and liquid slugs lengths on mass transport in the Taylor flow through capillaries. Chemical Engineering Science 52, 3709–3719.

Bothe, D., Koebe, M., Wielage, K., Warnecke, H.J., 2003. VOF-simulations of mass transfer from single bubbles and bubble chains rising in aqueous solutions. In: Proceedings of the Fourth ASME—JSME Joint Fluids Engineering Conference, Honolulu, Hawaii, USA, July 6–11, 2003.

Bothe, D., Koebe, M., Wielage, K., Prüss, J., Warnecke, H.J., 2004. Direct numerical simulation of mass transfer between rising gas bubbles and water. In: Sommerfeld, M. (Ed.), Bubbly Flows. Analysis, Modelling and Calculation. Springer, Berlin, pp. 159–174.

Crank, J., 1994. The Mathematics of Diffusion. second ed. Clarendon Press, Oxford.

Darmana, D., Deen, N.G., Kuipers, J.A.M., 2006. Detailed 3D modeling of mass transfer processes in two-phase flows with dynamic interfaces. Chemical Engineering and Technology 29, 1027–1033.

Davidson, M.R., Rudman, M., 2002. Volume-of-fluid calculation of heat or mass transfer across deforming interfaces in two-fluid flow. Numerical Heat Transfer B 41, 291–308.

Drew, D.A., Passman, S.L., 1999. Theory of Multicomponent Fluids. Springer, Berlin.

Elperin, T., Fominykh, A., 1999. Combined mass and heat transfer during nonisothermal absorption in gas–liquid slug flow with small bubbles in liquid plugs. International Journal of Heat and Mass Transfer 42, 153–163.

Elperin, T., Fominykh, A., 2003. Model of gas absorption in gas–liquid plug flow with first-order and zero-order chemical reaction. Heat and Mass Transfer 39, 195–199.

Gartsman, A.N., Cherkashin, V.V., Rassadnikova, N.N., 1979. Diffusion flux through a spherical gas–liquid interface in the presence of a chemical reaction in the liquid phase. International Chemical Engineering 19, 356–360.

Ghidersa, B., Wörner, M., Cacuci, D.G., 2004. Exploring the flow of immiscible fluids in a square vertical mini-channel by direct numerical simulation. Chemical Engineering Journal 101, 285–294.

Ghosh, R., Cui, Z.F., 1999. Mass transfer in gas-sparged ultrafiltration: upward slug flow in tubular membranes. Journal of Membrane Science 162, 91–102.

Hasegawa, Y., Kasagi, N., 2006. Effects of interfacial velocity boundary condition on turbulent mass transfer at high Schmidt numbers. In: Hanjalic, K., Nagano, Y., Jakirlic, S. (Eds.), Turbulence, Heat and Mass Transfer, vol. 5. Begell House, pp. 1–11.

Heiszwolf, J.J., Kreutzer, M.T., van den Eijnden, M.G., Kapteijn, F., Moulijn, J.A., 2001. Gas–liquid mass transfer of aqueous Taylor flow in monoliths. Catalysis Today 69, 51–55.

Hessel, V., Angeli, P., Gavriilidis, A., Löwe, H., 2005. Gas–liquid and gas–liquid–solid microstructured reactors: contact principles and applications. Industrial & Engineering Chemistry Research 44, 9750–9769.

Horvath, C., Solomon, B.A., Engasser, J.-M., 1973. Measurement of radial transport in slug flow using enzyme tubes. Industrial & Engineering Chemistry Fundamentals 12, 431–439.

Irandoust, S., Andersson, B., 1988. Mass transfer and liquid phase reactions in a segmented two-phase flow monolithic catalyst reactor. Chemical Engineering Science 43, 1983–1988.

Irandoust, S., Andersson, B., 1989. Simulation of flow and mass transfer in Taylor flow through a capillary. Computers & Chemical Engineering 13, 519–526.

Irandoust, S., Andersson, B., Bengtsson, E., Siverström, M., 1989. Scaling up of a monolithic catalyst reactor with two-phase flow. Industrial & Engineering Chemistry Research 28, 1489–1493.

Koynov, A., Khinast, J.G., 2006. Micromixing in reactive, deformable bubble, and droplet swarms. Chemical Engineering & Technology 29, 13–23.

Koynov, A., Khinast, J.G., Trygvasson, G., 2005. Mass transfer and chemical reactions in bubble swarms with dynamic interfaces. A.I.Ch.E. Journal 51, 2786–2800.
Kreutzer, M.T., Du, P., Heiszwolf, J.J., Kapteijn, F., Moulijn, J.A., 2001. Mass transfer characteristics of three-phase monolith reactors. Chemical Engineering Science 56, 6015–6023.
Kreutzer, M.T., Kapteijn, F., Moulijn, J.A., Heiszwolf, J.J., 2005. Multiphase monolith reactors: chemical reaction engineering of segmented flow in microchannels. Chemical Engineering Science 60, 5895–5916.
Ohta, M., Suzuki, M., 1996. Numerical analysis of mass transfer from a free motion drop in a solvent extraction process. Solvent Extraction Research and Development 3, 138–149.
Onea, A., 2006. Numerical simulation of mass transfer with and without first order chemical reaction in two-fluid flows. Ph.D. Thesis, University of Karlsruhe, Germany. Available at: ⟨http://digbib.ubka.uni-karlsruhe.de/eva/2007/maschinenbau/7t⟩.
Onea, A., Wörner, M., Cacuci, D.G., 2007. Numerical investigation of interfacial mass transfer in bubble train flow within square and rectangular mini-channels. In: Proceedings of the Sixth International Conference on Multiphase Flow (CD-ROM), July 9–13, 2007, Leipzig, Germany.
Özkan, F., Wörner, M., Wenka, A., Soyhan, H.S., 2007. Critical evaluation of CFD codes for interfacial simulation of bubble-train flow in a narrow channel. International Journal for Numerical Methods in Fluids 55, 537–564.
Paschedag, A.R., Piarah, W.H., Kraume, M., 2002. Treatment of limits for mass transfer at single droplets—validation of numerical results. Chemical Engineering & Technology 25, 953–956.
Paschedag, A.R., Piarah, W.H., Kraume, M., 2005. Sensitivity study for the mass transfer at a single droplet. International Journal of Heat and Mass Transfer 48, 3402–3410.
Patankar, S.V., 1980. Numerical Heat Transfer and Fluid Flow. Taylor and Francis, London. p. 45.
Petera, J., Weatherley, L.R., 2001. Modelling of mass transfer from falling droplets. Chemical Engineering Science 56, 4929–4947.
Pohorecki, R., Sobieszuk, P., Kula, K., Moniuk, W., Zieliński, M., Cygański, P., Gawiński, P., 2008. Hydrodynamic regimes of gas–liquid flow in a microreactor. Chemical Engineering Journal 135S, S185–S190.
Radl, S., Tryggvason, G., Khinast, J.G., 2007. Flow and mass transfer of fully resolved bubbles in non-Newtonian fluids. A.I.Ch.E. Journal 53, 1861–1878.
Sabisch, W., Wörner, M., Grötzbach, G., Cacuci D.G., 2001. 3D Volume-of-fluid simulation of a wobbling bubble in a gas-liquid system of low Morton number. In: Proceedings of the fourth International Conference on Multiphase Flow (CD-ROM), May 27–June 1, New Orleans, LA, USA.
Sander, R., 1999. Modeling atmospheric chemistry: interactions between gas-phase species and liquid cloud/aerosol particles. Surveys in Geophysics 20, 1–31.
Sato, T., Jung, R.-T., Abe, S., 2000. Direct simulation of droplet flow with mass transfer at interface. ASME Journal Fluids Engineering 122, 510–516.
Thulasidas, T.C., Abraham, M.A., Cerro, R.L., 1995. Bubble-train flow in capillaries of circular and square cross-section. Chemical Engineering Science 50, 183–199.
Thulasidas, T.C., Abraham, M.A., Cerro, R.L., 1997. Flow patterns in liquid slugs during bubble-train flow inside capillaries. Chemical Engineering Science 52, 2947–2962.
Toor, H.L., Marchello, J.M., 1958. Film-penetration model for mass and heat transfer. A.I.Ch.E. Journal 4, 97–101.
Tsoligkas, A.N., Simmons, M.J.H., Wood, J., 2007a. Influence of orientation upon the hydrodynamics of gas–liquid flow for square channels in monolith supports. Chemical Engineering Science 62, 4365–4378.
Tsoligkas, A.N., Simmons, M.J.H., Wood, J., 2007b. Two-phase gas–liquid reaction studies in a circular capillary. Chemical Engineering Science 62, 5397–5401.
Tsoligkas, A.N., Simmons, M.J.H., Wood, J., Frost, C.G., 2007c. Kinetic and selectivity studies of gas–liquid reaction under Taylor flow in a circular capillary. Catalysis Today 128, 36–46.
van Baten, J.M., Krishna, R., 2004. CFD simulations of mass transfer from Taylor bubbles rising in circular capillaries. Chemical Engineering Science 59, 2535–2545.
van Baten, J.M., Krishna, R., 2005. CFD simulations of wall mass transfer for Taylor flow in circular capillaries. Chemical Engineering Science 60, 1117–1126.
Vandu, C.O., Liu, H., Krishna, R., 2005. Mass transfer from Taylor bubbles rising in single capillaries. Chemical Engineering Science 60, 6430–6437.
Waheed, M.A., Henschke, M., Pfennig, A., 2002. Mass transfer by free and forced convection from single spherical liquid drops. International Journal of Heat and Mass Transfer 45, 4507–4514.
Whitaker, S., 1973. The transport equations for multi-phase systems. Chemical Engineering Science 28, 139–147.
Whitaker, S., 1999. The Method of Volume Averaging. Kluwer Academic Publishers, Dordrecht.
Wörner, M., Sabisch, W., Grötzbach, G., Cacuci, D.G., 2001. Volume-averaged conservation equations for volume-of-fluid interface tracking. In: Proceedings of the Fourth International Conference on Multiphase Flow (CD-ROM), May 27–June 1, New Orleans, LA, USA.
Wörner, M., Ghidersa, B., Onea, A., 2007. A model for the residence time distribution of bubble-train flow in a square mini-channel based on direct numerical simulation results. International Journal of Heat and Fluid Flow 28, 83–94.
Yang, C., Mao, Z.-S., 2005. Numerical simulation of interphase mass transfer with the level set method. Chemical Engineering Science 60, 2643–2660.
Yue, J., Chen, G., Yuan, Q., Luo, L., Gonthier, Y., 2007. Hydrodynamics and mass transfer characteristics in gas–liquid flow through a rectangular microchannel. Chemical Engineering Science 62, 2096–2108.
Zheng, D., Che, D., 2007. An investigation on near wall transport characteristics in an adiabatic upward gas–liquid two phase slug flow. Heat and Mass Transfer 43, 1019–1036.